HELICOPTER TAIL BOOM VIBRATION ANALYSIS AND SUPPRESSION

M.E.Funnell

Thesis presented in partial fulfilment of the requirements for the degree Master of Science in Engineering at the University of Stellenbosch

Thesis Supervisor: Dr D. Pienaar

March 2002

DECLARATION

I, the undersigned, hereby declare that the work contained in this thesis is my own original work and that I have not previously in its entirety or in part submitted it at any university for a degree.

Signature Date

ABSTRACT

An experimental investigation was conducted using a cantilever beam to illustrate an understanding of vibration techniques and phenomena. The free and forced vibration of the cantilever beam was investigated using various modelling strategies. Theoretical models such as the Lumped parameter, Myklestad, Distributed Parameter and Finite Element Methods were analysed and compared with experimental measurements. Excellent agreement of the natural frequencies, mode shapes and the harmonic transfer functions were found.

To investigate tail boom vibration, a Finite Element Model of a simplified helicopter tail boom design was tested against experimentally measured data. The results correlated accurately and the model was used to evaluate the effectiveness of a vibration suppression system designed for the tail boom.

The vibration suppression system was designed using two, parallel dynamic absorbers to reduce tail boom vibrations at its two dominant frequencies. For the purposes of this thesis, the dynamic absorbers were tuned to reduce the resonant peaks at the dominant excitation frequencies of the excitation force in-line with the thrust of the tail rotor only. This excitation force was estimated using a simplified tail rotor dynamic model, which when compared with actual vibration data was assumed to predict the basic frequency trends of the force, reliably. Incorporating the designed components into an accurate Lumped Parameter model of a cantilever beam structure and simulating the response of the structure at the dominant excitation frequencies of the calculated excitation force, tested the vibration suppression system. The results of this investigation proved the effectiveness of the design procedure and optimisation process of the design parameters. A similarly designed suppression system was incorporated into the Finite Element tail boom model and from the analytical results obtained it was shown to cause a fair reduction in the vibration response at the two dominant frequencies of the excitation force.

Finally, two possible applications were suggested from the research presented in this thesis. The first application was the simplified configuration of a vibration monitoring system for the tail boom. The second application was the possible development of a system using the response of vibration suppression absorbers to predict the magnitudes of the excitation forces on the tail boom.

OPSOMMING

'n Experimentele ondersoek is onderneem deur gebruik te maak van 'n ingeklemde balk om vibrasie tegnieke te illustreer. Die vrye en geforseerde vibrasie van die ingeklemde balk is ondersoek deur verskillende model tegnieke te gebruik. Teoretiese modelle soos die Lumped parameter, Myklestad, Distributed Parameter en Eindige Element Metodes was geanaliseer en vergelyk met die eksperimentele waardes. Uitstekende ooreenstemmings was gevind tussen die natuurlike frekwensies, die eievektore en die harmoniese oordragsfunksie.

Om stert vibrasie te ondersoek, was'n eindige element model van 'n helikopter stert getoets teenoor die eksperimentele data. Die resultate het akuraat gekorreleer en dus was die model gebruik om die effektiwiteit van 'n vibrasie supressie sisteem te evalueer.

Die vibrasie supressie sisteem was ontwerp deur gebruik te maak van twee parallele dinamiese absorbeerders om die helikopter stert se eerste twee dominante vibrasie frekwensies te minimeer. Vir die doel van hierdie tesis was die dinamiese absorbeerders ingestel om net die resonante pieke van die opgewende krag wat in lyn is met die drykrag van die stert rotor te minimeer. Hierdie opgewende krag was, deur gebruik te maak van 'n basiese stert rotor dinamiese model, aanvaar om die basiese frekwensie tendense van die krag te voorspel. Die supressie sisteem wat ontwerp was, was getoets op die lumped parameter balk en het veroorsaak dat die voorspelde opgewende krag by al twee van sy dominante frekwensies baie geminimeer was. Die effektiwiteit van die sisteem was dus bewys en die sisteem was gebruik om die respons van die eindige element model van die stert te verbeter. Die resultate het 'n aanvaarbare reduksie in die respons by die twee dominante frekwensies van die opgewende krag, gewys.

Laastens, deur gebruik te maak van die resultate in hierdie tesis, was twee moontlikhede voorgestel. Die eerste een was die konfigurasie van 'n vibrasie moniterings sisteem vir die helikopter stert. Die tweede mmontlikheid was die moontlike ontwikkeling van 'n sisteem wat die grootte van die opgewende krag by die stert rotor kon voorspel, deur gebruik te maak van die vibrasie suppressie absorbeerders.

ACKNOWLEDGEMENTS

The following people are thanked for their help in producing this thesis:

Dr. D Pienaar for his insight and guidance throughout the development of the thesis

Mr. K. Van der Westhuizen for his help with finite element modelling aspects

TABLE OF CONTENT

LIST OF TABLES

LIST OF FIGURES

NONMENCLATURE

Vectors, Matrices and Functions

Column Vectors are represented by the over-bar symbol

$\bar{a}$	Acceleration Vector
$[A]$	Flexibility Matrix
$\bar{c}$	Spatial constants vector
$[C]$	Damping Matrix
$[D]$	Frequency Matrix
$\bar{F}, \bar{f}$	Force Vector
$h(\omega)$	Harmonic Transfer Function
$[H]$	Harmonic Transfer Matrix
$[K]$	Stiffness Matrix
$[M]$	Mass Matrix
$P(x)$	Penalty Function
$q(t)$	Temporal Function
$[T]$	Myklestad Matrix
$\bar{u}$	Eigenvector
[U]	Eigenvector Matrix
$\bar{W}, \bar{w}$	Displacement Vector
$\phi(x)$	Pseudo-objective Function
$\varphi(x)$	Spatial Function
$[\lambda]$	Spectral Matrix

Scalars

a	Lift Curve Slope of Blade, Acceleration
A	Area
b	Number of Blades
c	Chord Length, Damping, Constant Terms
D_o	Equivalent Flat-plate Area of Helicopter
E	Young's Modulus
f	Force, Distributed Loading on a Beam
I	Second Moment of Area

k, K	Stiffness
l, L	Length
m, M	Mass, Moment
n	Number of Lumped Segments
N	Rotation Speed [rpm]
p	Penalty Multiplier
q, Q	Torque
r	Radius
R	Reaction Forces at the Blade Hinge, Radius
s	Solidity
t	Time
U, V	Fourier Series Components of the Reaction force at the Hinge, Velocity
u, w	Displacement
v_i	Induced Velocity
V_{ff}	Air Speed
W	Weight of Helicopter
x	Distance Along Beam
Z	Non-Rotating Excitation Force
α	Mass Coefficient of Proportional Damping, Main Rotor Incidence
β	Stiffness Coefficient of Proportional Damping Flapping angle of Blade
$\beta_0, A_\beta, B_\beta$	Steady State Flapping Coefficients
δ	Profile-Drag Coefficient
ϕ	Inflow Angle
γ	Poisons Ratio, Lock's Number
λ_i	Inflow Ratio
μ	Advance Ratio
θ	Rotation, blade twist
ρ	Density
ς	Damping Ratio

ω	Angular Velocity
Ω	Rotation Speed [rad/s]
ψ	Rotation Angle

Superscripts

b	Body Fixed Base
f	Force
h	Rotating Base
H	Non-rotating Base
l	Left Hand Side
M	Moment
R	Right Hand Side

Subscripts

a	Absorber
b	Blade
c	Coefficient
cg	Centre of Gravity
D	Disc-Axis
dr	Driving
eff	Effective
eq	Equivalent
f	Field
$flex$	Flexibility
i	Induced
n	Natural
s	Station

1 INTRODUCTION

"Helicopter Vibrations is a problem long-standing. From the earliest days of rotorcraft development, oscillatory motion of the non-rotating portion of the airframe has been a matter of serious concern, and from several viewpoints. Oscillatory motion usually means oscillatory strain – since rigid body motion is rarely the major component of motion at the frequencies of interest – and oscillatory strain often involves fatigue of structural components, with concomitant reduced availability and increased maintenance cost. Similarly, vibrations constitute a hostile environment for equipment of all kinds. They make instruments hard to read, sight hard to aim, weapons hard to point and the add to fatigue of pilots, crew and passengers." – Loewy[1]

Although the tail rotor causes a lesser effect then the main rotor on the overall vibration of the helicopter, its effects cannot be neglected. In order to develop an improved understanding of tail boom vibration and suggest methods of reducing vibration levels and monitoring tail rotor vibrations, a research project was undertaken with the following main objectives:

- To obtain an advanced understanding of analytical and experimental vibration analysis techniques and phenomena.
- To analyse tail boom vibrations using an accurate Finite Element Model of a simplified tail boom structure.
- To design a vibration suppression system which reduces tail boom vibrations at the two dominant lateral vibration frequencies.
- To suggest possible applications of the researched results.

1.1 VIBRATION ANALYSIS

A simple cantilever beam is analysed using various modelling strategies and compared to experimental data to obtain an understanding of vibration analysis techniques and procedures. Modal analysis, as presented by Ewins[2], is used to identify natural frequencies and related modes of the structure and is assumed an effective and thorough technique for analysing model effectiveness. The modes are characteristic shapes associated with particular resonant frequencies. The shapes and frequencies are dependent on the mass, stiffness and damping properties of the entire structure and are the building blocks of the response of the structure.

Numerous discrete and continuous modelling strategies are available to analyse the free and forced response of beam structures. From the comparative formulations given in Tse, Morse & Hinkle[3], Meirovich[4] and Inmann[5], the Myklestad, Lumped Parameter and Distributed Parameter modelling strategies were selected.
As stated by Tse, Morse & Hinkle[3], the Myklestad method uses a tabular method to determine modes and natural frequencies of structures and is commonly used to analyse aeroplane wings.

The continuous modelling strategy provides an exact solution for the beam response and is commonly used to analyse beam structures with various attachments and clamping conditions. Rossit & Laura[6], analysed the free vibration of a cantilever beam with a spring mass system attached to the free end, using the Euler-Bernoulli beam theory. Low[7], compares experimental and numerical frequencies of Euler-Bernoulli beams, carrying a mass in-span, with various clamping conditions.

As stated by Loewy[1], Finite Element analysis of the helicopter fuselage has become a way of life for vibration groups. The details of the Finite Element Modelling strategy are found in Cook, Malkus & Plesha [8]. Yeo & Chopra[10] and Fledel, Rand & Chopra[9] present coupled rotor/airframe vibration analyses using the finite element approach.

1.2 TAIL BOOM VIBRATION ANALYSIS

To evaluate helicopter tail boom vibrations, a simplified tail boom test structure is designed and modelled using the Finite Element Modelling Strategy. Accurate calculation of the required natural frequencies, mode shapes and frequency transfer functions is difficult due to the complex structure of the helicopter fuselage. Bramwell[11], pg. 350 , states that reliable approximations can nevertheless be obtained by modelling the fuselage as an assembly of elements having certain masses and stiffness, and assuming the response will correspond to a horizontal 'free-free' beam. The finite element model can be used as a virtual testing environment to predict tail boom responses during specific flight patterns and to evaluate the effectiveness of vibration suppression systems without the necessity of in-flight or experimental testing.

1.3 VIBRATION SUPPRESSION

For the purposes of this thesis, a vibration suppression system is designed using dynamic absorbers to counteract the lateral force that acts in-line with the thrust of the tail rotor only. A reliable prediction of the excitation frequencies of the dynamic forces requires the development of a tail rotor dynamic analysis. Bramwell[11] and Gessow & Myers[12] present dynamic theories and aerodynamic principles, used mainly for the analysis of the main rotor and based on the fundamental works of Glauert and Lock. These dynamic theories, however, in a simplified version with no lag motion, are directly applicable to tail rotor analysis. The extended Euler equations of rigid body rotation and definitions of particle acceleration used in the analyses are derived by Greenwood[13].

Tse, Morse & Hinkle[3] and Inman[5] analyze the effectiveness of single degree of freedom, damped and undamped vibration absorbers, using conventional mass-spring-damper systems. They show methods for deriving response equations of systems with a single dynamic vibration absorber and discuss the design parameters attributed to these responses. Cha & Pierre[14] studied the effect of a chain of mass-spring oscillators on the frequency response of a linear elastic structure, using the assumed modes method to define the free vibration of the structure. Aida et al[15] investigated vibration control of beams using beam-type dynamic vibration absorbers. They found that the equations of motion in the modal co-ordinates of the main beam were equivalent to modelling the beam structures as single degree of freedom mass-spring systems.

1.4 MONITORING SYSTEMS

Continuous in-flight monitoring systems form part of a relatively new development called Health and Usage Monitoring Systems or HUMS. The development of a complex vibration monitoring system is outside the scope of this thesis. A simplified monitoring system is however investigated using the basic configuration and requirements of HUMS components presented by Muldoon & Gill [16], Blunt, O'Neill & Rebbechi [17] and Trammel[18].

2 VIBRATION ANALYSIS

The free and forced vibration of a slender cantilever beam is investigated using the Lumped Parameter, Myklestad, Distributed Parameter and Finite Element Modelling strategies. The results are compared with experimental measurements to test the reliability of the analytical models. The investigation provides an advanced understanding of vibration analysis procedures and gives insight in vibration phenomena.

2.1 TEST STRUCTURE

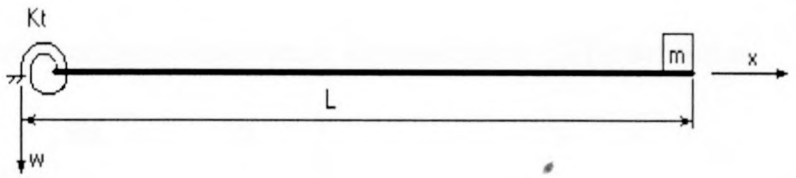

Figure 2.1-1: Cantilever Test Model

Analytical models are developed for a non-tapering cantilever beam structure with a tip mass and a stiff torsional spring modelling the clamping stiffness, as shown in Figure 2.1-1. The vibration theories are formulated using the Euler-Benoulli beam theory due to the slender nature of the beam. The clamping spring stiffness K_t and the effective bending stiffness EI are calculated from the static deflection of the beam under an applied load, as described in Appendix A.1.

2.1.1 Lumped Parameter Model

The Lumped Parameter method is physically motivated and amounts to lumping distributed mass at given points in the domain of the system. The stiffness is not lumped but described in this case by means of influence coefficients, thus regarding them as distributed across the section. In this way, a system could be modelled as a multiple degree of freedom system, providing general solutions to quite complex problems. The accuracy of results depends on the number and length of the increments the system is divided into. This type of mass lumping is illustrated in Figure 2.1-2, taken from Inmann[5].

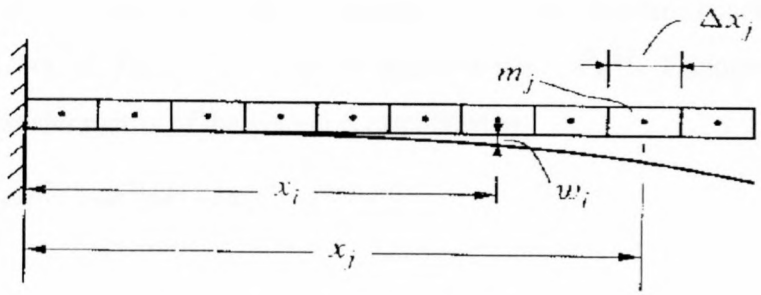

Figure 2.1-2: Mass Lumping of Cantilever Beam

The equations of motion are derived from Newton's law as:

$$[M]\ddot{\bar{w}}+[C]\dot{\bar{w}}+[K]\bar{w} = \bar{f}(t) \qquad \text{[2.1.1-1]}$$

For n lumped sections of equal mass, the mass matrix $[M]$ is defined as

$$[M] = \begin{bmatrix} \partial m & \cdots & 0 \\ \vdots & \ddots & \vdots \\ 0 & \cdots & \frac{1}{2}\partial m + m_{tip} \end{bmatrix} \qquad \text{[2.1.1-2]}$$

$$\partial m = M_{beam}/n$$

The stiffness matrix $[K]$ is calculated from the derivation of the flexibility matrix $[A]$ of the beam as shown in Appendix A.2, where,

$$[K] = [A]^{-1} \qquad \text{[2.1.1-3]}$$

The damping matrix is assumed proportional to the mass and stiffness of the beam and is defined as

$$[C] = \alpha[M] + \beta[K] \qquad \text{[2.1.1-4]}$$

The coefficients α and β are calculated using data from the experimental estimation of the damping of the system as described in Appendix A.3.2.

The un-damped natural frequencies of the system, the eigen-value problem of the system is solved using the MATLAB *eig* function as:

$$[U,\lambda] = eig([K],[M]) \qquad \text{[2.1.1-5]}$$

$[U]$ is the matrix of eigenvectors of the system

$[\lambda]$ is the spectral matrix

For harmonic excitation, the beam is assumed to react in a similar manner to the applied force, therefore, if $\bar{f}(t) = \overline{F}e^{i\omega t}$ then the response is $w = \overline{W}e^{i\omega t}$. Factoring out $e^{i\omega t}$, the harmonic transfer matrix of the system is calculated as

$$[H(\omega)] = (-\omega^2[M] + i\omega[C] + [K])^{-1} \qquad [2.1.1\text{-}6]$$

For an applied harmonic force at the end of the beam, the transfer function measuring the displacement at the end of the beam, is defined as:

$$h(\omega) = H_{nn}(\omega) \qquad [2.1.1\text{-}7]$$

2.1.2 Myklestad Model

The Myklestad method is also a lumped parameter approach, where a typical segment consists of a massless span and a point mass. The elastic properties are described by a field transfer matrix $[T_f]$ of the span and the inertial effects by a station transfer matrix $[T_s]$ of the mass. Tse, Morse & Hinkle[3] define these as:

$$[T_{si}] = \begin{bmatrix} 1 & 0 & 0 & 0 \\ 0 & 1 & 0 & 0 \\ 0 & 0 & 1 & 0 \\ -\omega^2 m_i & 0 & 0 & 1 \end{bmatrix} \qquad [2.1.2\text{-}1]$$

$$[T_{fi}] = \begin{bmatrix} 1 & \partial x_i & w_i^M & \left(w_i^f - \partial x_i w_i^M\right) \\ 0 & 1 & \theta_i^f & \left(\theta_i^f - \partial x_i \theta_i^M\right) \\ 0 & 0 & 1 & -\partial x_i \\ 0 & 0 & 0 & 1 \end{bmatrix} \qquad [2.1.2\text{-}2]$$

m_i represents the mass at station i

∂x_i represents the incremental lumping divisions of field i

w_i^M represents the displacement at $i+1$ due to a unit moment at $i+1$, regarding station i as fixed.

θ_i^M represents the rotation at $i+1$ due to a unit moment at $i+1$, regarding station i as fixed.

w_i^f represents the displacement at $i+1$ due to a unit force at $i+1$, regarding station i as fixed.

θ_i^f represents the rotation at $i+1$ due to a unit force at $i+1$, regarding station i as fixed.

The displacement and rotation components of the field matrix are calculated from simple beam theory, as described in Appendix A.2. According to the Myklestad approach, the Eigenvalue problem is derived in a step-by-step process, advancing from one end of the member to the other. The equations of motion are therefore defined by Tse Morse and Hinkle[3] as:

$$\begin{Bmatrix} w \\ \theta \\ M \\ f \end{Bmatrix}_{n+1}^{R} = [T(\omega)] \begin{Bmatrix} w \\ \theta \\ M \\ f \end{Bmatrix}_{1}^{L} \qquad \text{[2.1.2-3]}$$

$$[T(\omega)] = [T_s]_{n+1} \Pi_{i=n}^{1} [T_f]_i [T_s]_i$$

The Myklestad method relies on the accurate representation of the boundary conditions of the system, which require that:

$$w_1^L = 0 \qquad \text{[2.1.2-4]}$$

$$\theta_1^L = M_1^L / K_t \qquad \text{[2.1.2-5]}$$

$$M_{n+1}^R = 0 \qquad \text{[2.1.2-6]}$$

$$f_{n+1}^R = 0 \qquad \text{[2.1.2-7]}$$

The $2x2$ frequency matrix is thus derived from the Myklestad matrix as

$$[D] = \begin{bmatrix} (T_{32}/K_t + T_{33}) & T_{34} \\ (T_{42}/K_t + T_{43}) & T_{44} \end{bmatrix} \qquad \text{[2.1.2-8]}$$

The Eigenvalue problem is solved using the Newton-Raphson numerical method, by setting the determinant of the frequency matrix to zero.

Substituting the appropriate natural frequency into the eigenvalue problem, and assuming unit force f_1^L, the eigenvector $\{M \quad f\}_1^{L^T}$ is calculated, where

$$M_1^L = -D_{12}/D_{11} \qquad [2.1.2\text{-}9]$$

This eigenvector is merely an element of the larger eigenvector $\{w \quad \theta \quad M \quad f\}_1^{L^T}$ at all stations, which can be calculated using the appropriate eigenvalues from station to station until the tip of the beam is reached.

For an applied harmonic force, with angular velocity ω at the end of the beam, the transfer function measuring the displacement at the end of the beam, is defined as:

$$h(\omega) = T_{12}M_1^L/K_t + T_{13}M_1^L + T_{14}f_1^L \qquad [2.1.2\text{-}10]$$

2.1.3 Distributed Parameter Model

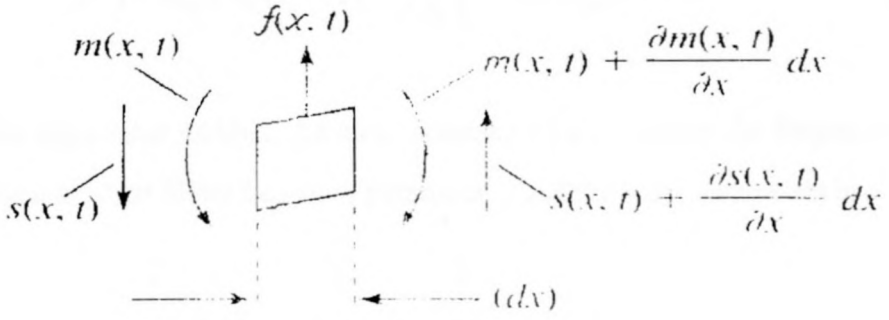

Figure 2.1-3: Differential element of Euler Bernoulli Beam bending

Figure 2.1-3 shows the differential element for the derivation of the Euler Bernoulli distributed parameter model. The forced vibration of an Euler Bernoulli beam in bending is therefore derived from the differential equation:

$$m\frac{\partial^2 w}{\partial t^2} + EI\frac{\partial^4 w}{\partial x^4} = f(x,t) \qquad [2.1.3\text{-}1]$$

For free vibration $f(x,t) = 0$ and the response is assumed to be composed of spatial $\varphi(x)$ and temporal $q(t)$ solutions.

Therefore letting $w(x,t) = \varphi(x)q(t)$ and using the 'technique of separation of variables', a general solution for the spatial solution is

$$\varphi = c_1 \cos(\beta x) + c_2 \cosh(\beta x) + c_3 \sin(\beta x) + c_4 \sinh(\beta x) \qquad \text{[2.1.3-2]}$$

$$\beta^4 = m\omega^2 / EI$$

The spatial equation is used to solve the eigenvalue problem, which is dependent on the boundary conditions of the system. Theses are expressed in terms of the spatial variable as follows:

Displacement at the clamped end is zero:

$$w(0) = 0 \therefore \varphi(0) = 0 \qquad \text{[2.1.3-3]}$$

Angular rotation at clamped end is defined by the properties of the torsional spring:

$$\theta(0) = M(0)/K_t \therefore EI\, \partial^2\varphi/\partial x^2\Big|_{x=0} - K_t\, \partial\varphi/\partial x\Big|_{x=0} = 0 \qquad \text{[2.1.3-4]}$$

Applied moment at the free end is zero:

$$M(l) = 0 \therefore EI\, \partial^2\varphi/\partial x^2\Big|_{x=l} = 0 \qquad \text{[2.1.3-5]}$$

Applied force at the free end is proportional to the acceleration of the accelerometer

$$f(l) = m_{tip}\, \partial^2 w/\partial t^2 \therefore EI\, \partial^3\varphi/\partial x^3\Big|_{x=l} + \omega^2 m_{tip}\varphi(l) = 0 \qquad \text{[2.1.3-6]}$$

The eigenvalue problem therefore becomes $[D]\bar{c} = \bar{0}$ where the frequency matrix $[D]$ is given in terms of the frequency parameter β and the beam parameters by:

$$[D] = \begin{bmatrix} 1 & 1 & 0 & 0 \\ -k_0\beta L & k_0\beta L & -1 & -1 \\ -\cos\beta L & \cosh\beta L & -\sin\beta L & \sinh\beta L \\ d_{41} & d_{42} & d_{43} & d_{44} \end{bmatrix} \qquad \text{[2.1.3-7]}$$

$$d_{41} = \sin\beta L + \mu_L \beta L \cos\beta L$$

$$d_{42} = \sinh\beta L + \mu_L \beta L \cosh\beta L$$

$$d_{43} = -\cos\beta L + \mu_L \beta L \sin\beta L$$

$$d_{44} = \cosh\beta L + \mu_L \beta L \sinh\beta L$$

$$k_o = EI/K_t L$$

$$\mu_L = m_{tip}/M_{beam}$$

The natural frequencies are calculated using the Newton-Raphson numerical method by setting the determinant of the frequency matrix $[D]$ to zero.

By setting $c_1 = 1$ and substituting the natural frequencies into the eigenvalue problem, the spatial coefficients c_2, c_3, c_4 can be derived, normalised w.r.t c_1. The eigenfunctions are derived from the spatial equation, using appropriate natural frequencies.

The undamped force response of the system is solved using the modal analysis technique described in Tse, Morse and Hinkle [3]. Using the temporal equation and the orthogonality properties of the Eigen functions (refer to Appendix A.4), the differential equation of the forced motion in the modal coordinates q_i are shown to be:

$$\hat{m}_i \ddot{q}_i + \hat{k}_i q_i = \int_0^L f(x,t)\varphi_i(x)dx = \hat{f}_i \qquad \text{[2.1.3-8]}$$

$$\hat{m}_i = m\int_0^L \varphi_i^2(x)dx + m_{tip}\varphi_i^2(L)$$

$$\hat{k}_i = EI\int_0^L \left(\varphi_i''(x)\right)^2 dx + K_t(\varphi_i'(0))^2$$

For harmonic excitation and force application at the end of the beam, the generalised force is defined as $\hat{f}_i = Fe^{jwt}\varphi_i(L)$. The beam is assumed to react in a similar manner to the applied force, therefore the response is $q_i = Q_i e^{j\omega t}$. Substituting these equations into equation 2.1.3-8 and factoring out $e^{j\omega t}$, the result yields

$$Q_i(-\omega^2\hat{m}_i + \hat{k}_i) = F_i \qquad \text{[2.1.3-9]}$$

Q_i is the modal magnitude of the harmonic response for the $i-th$ mode

F_i is the modal magnitude of the harmonic force for the $i-th$ mode

The modal coordinates are transformed into actual coordinates using the relationship $w(x,t) = \sum_{i=1}^{\infty}\varphi_i(x)q_i(t)$. The harmonic transfer function, measuring deflection at the end of the beam caused by a force applied at the same point, is therefore defined as:

$$h(\omega) = \sum_{i=1}^{\infty}\left(\frac{\varphi_i(L)\varphi_i(L)}{\left(-\omega^2\hat{m}_i + \hat{k}_i\right)}\right) \qquad \text{[2.1.3-10]}$$

2.1.4 FEM Model

Msc/NASTRAN for windows is used as the format for the required FE model and analysis thereof. The slender beam is modelled using BEAM- elements and the fixture is modelled using the torsional property of the SPRING-element in the NASTRAN element library. The beam dimensions are given from the technical drawings of the test structure, with stress releases incorporated at each BEAM-element corner. The tip mass is modelled as a concentrated MASS element at the end of the beam.

2.1.5 Experimental Procedures

2.1.5.1 Estimation of Modes Shapes, natural frequencies and damping

The methods used to derive the mode shapes and damping ratios of the experimental test structure are derived in Appendix A.3. Natural frequencies are formulated from the peak frequencies of the transfer functions.

2.1.5.2 Instrumentation and Calibration

ITEM	MANUFACTURER	MODEL
PCB Accelerometers	Piezotronics	353B15
Force Transducer	Bruel and Kjæl	8200
Shaker	Bruel and Kjæl	
Power Amplifier	Bruel and Kjæl	2706
Charge Amplifier	Bruel and Kjæl	2635
SigLab	DSP technology	20-42

Table 2.1-1: Experimental Equipment List

Table 2.1-1 lists the various items used in the experimental testing process. The accelerometers measure response at specific points on the beam and are set using the manufacturer's calibration factors. The input signal is generated by the SIGLAB system and amplified through the power amplifier. The force transducer measures the input force and is amplified through the charge amplifier.

2.1.6 Experimental and Analytical Results

The Lumped Parameter, Myklestad and Distributed Parameter formulations are simulated in MATLAB using the beam properties given in Appendix A.5.

Exciting the structure and measuring the input forces and output structural response using the accelerometers accomplished experimental measurements. The accelerometers are placed at 10 evenly distributed positions along the beam and the response is measured relative to a random input force at the end of the beam. The measured frequency response functions between points of random force application and response measurement and the corresponding coherence data are calculated and stored using SIGLAB software.

The frequency response function allows calculation of the mode shapes, natural frequencies and the modal damping ratios using the experimental methods derived in Appendix A.3. The coherence function provides a means of checking measurement accuracy so that unacceptable data can be re-sampled. A bandwidth of 200 Hz with a sampling window of 1024 points was selected for the test. The excitation range of 0 to 200 Hz was used, corresponding to the acquisition frequency range. Appendix A.6 illustrates the accelerometer and shaker set-up, the amplifier set-up and the SIGLAB system used during the test procedure.

The natural frequencies obtained from the analytical models are compared with the experimental results in Table 2.1-2. All four models correlate accurately at the first frequencies, with the three lumped models (Lumped parameter, Myklestad and FEM), producing very similar results. At the second natural frequencies, the lumped models become less reliable, but the distributed parameter model still correlates accurately with the experimental results.

The first two mode shapes of the cantilever beam are compared in Figures 2.1-4 and 2.1-5. The three lumped techniques produce very similar results and the distributed parameter model differs only slightly form these. The experimental mode shapes correlate accurately with the analytical mode shapes.

The transfer functions measured at the end of the beam are given in figure 2.1-6 with the corresponding experimental coherence data in figure 2.1-7. The coherence data proves the reliability of the obtained transfer function, with the only unreliable data situated in the low frequency ranges. This is mainly due to the effects external low frequency sources on the experimental data and the low reliability of the accelerometers at low frequencies. The transfer functions illustrate the first two resonance peaks and the anti-resonance peaks of the beam. The resonance peaks of all the strategies correlate fairly accurately with the experimental regions. The distributed parameter model correlates more accurately at the higher frequencies (>120Hz) then the approximate models.

Figure 2.1-8 provides a visual close up of the first and second frequency peaks relative to the experimental results to substantiate the above statements. The analysis of the peaks reveals the effect of damping on the beam transfer functions. The undamped peaks associated with the Myklestad and Continuous models are sharper and higher than the damped peaks associated with the FE analysis and experimental data. Note that the undamped resonance peaks are theoretically infinite, but are shown finite because of the resolution of the data points on the graph. The peak values of the lumped parameter and finite element models, which incorporates the experimentally calculated damping ratios, show a fair correlation with the damped experimental frequencies.

The results prove the accuracy of all four modelling strategies and of the calculation of the experimental damping ratios and mode shapes from the experimental measurements. The analysis gives a thorough background into vibration analysis techniques and highlights the most important vibration phenomena. Thus it is useful guide to understanding the vibration problems, which may occur during the analysis of the more complex tail boom structure.

Natural Frequency	Lumped Parameter Model (Hz)	Distributed Parameter Model (Hz)	Myklestad Model (Hz)	Finite Element model (Hz)	Experimental Results (Hz)
1st	21.3524	21.4249	21.3517	21.3582	21.3273
2nd	144.4093	146.0992	144.4092	144.4635	147.8023

Table 2.1-2: Comparison of Natural Frequencies of Slender Beam

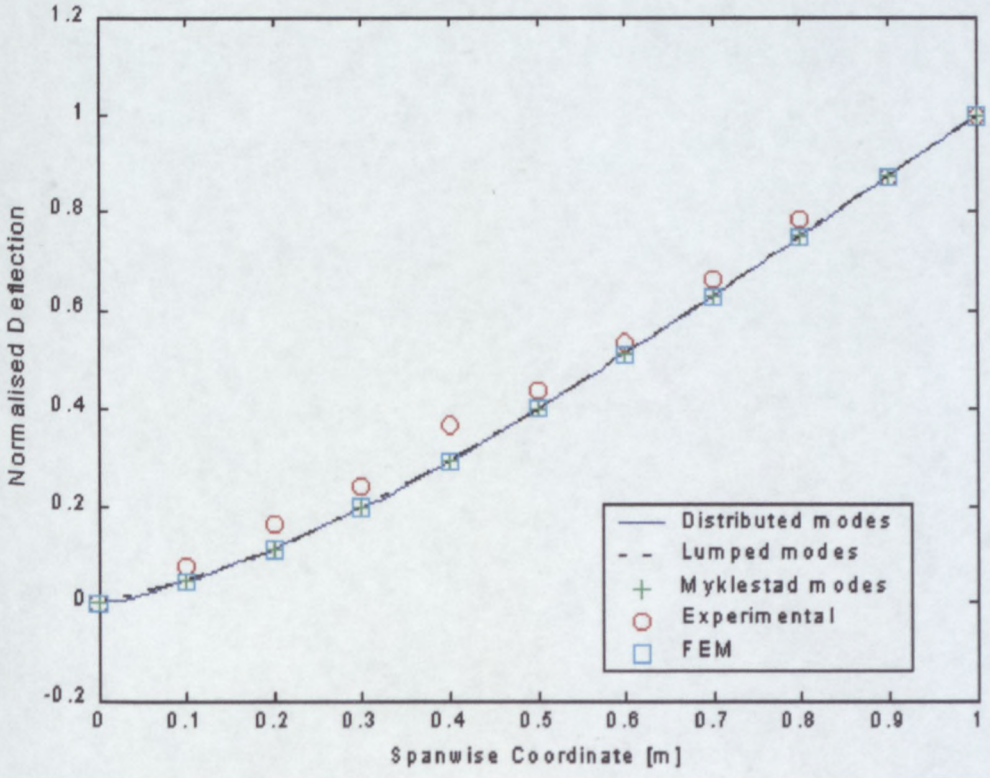

Figure 2.1-4: Comparison of 1st Mode Shape of Slender beam

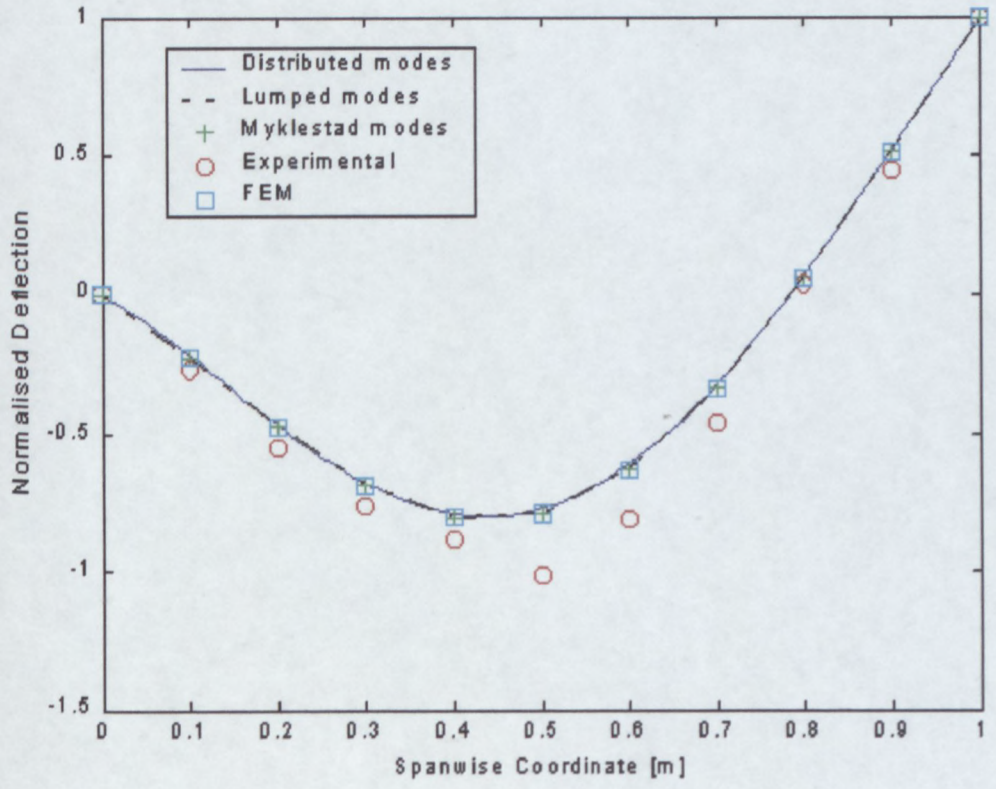

Figure 2.1-5: Comparison of 2nd Mode Shape of Slender Beam

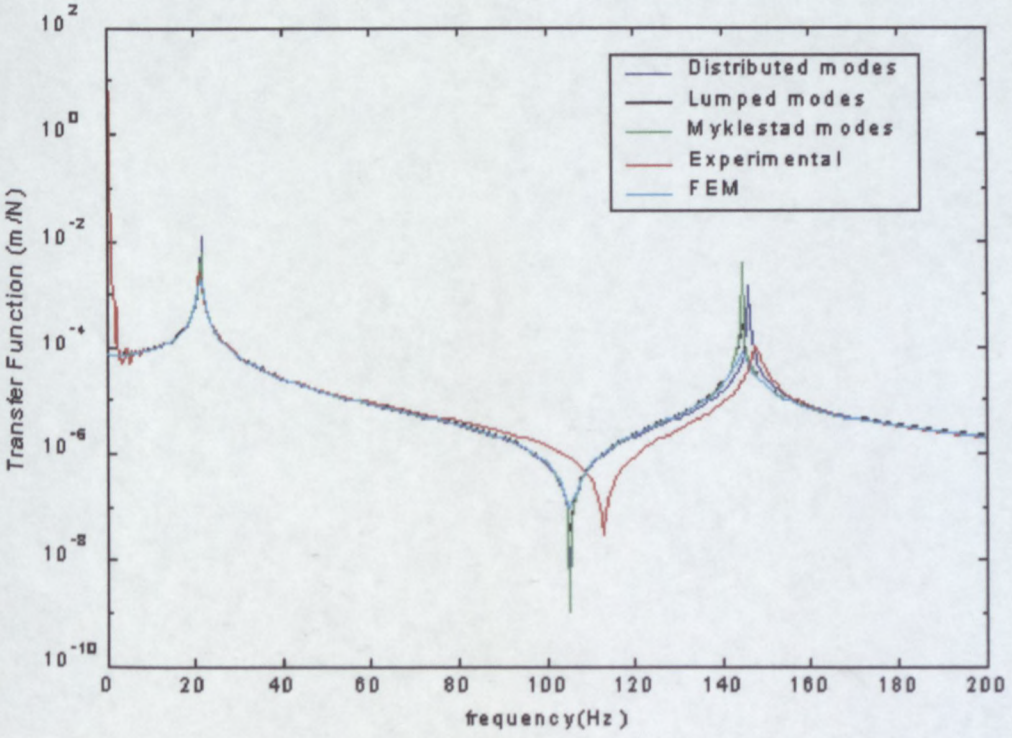

Figure 2.1-6: Predicted and Measured Tip to Tip Transfer Function

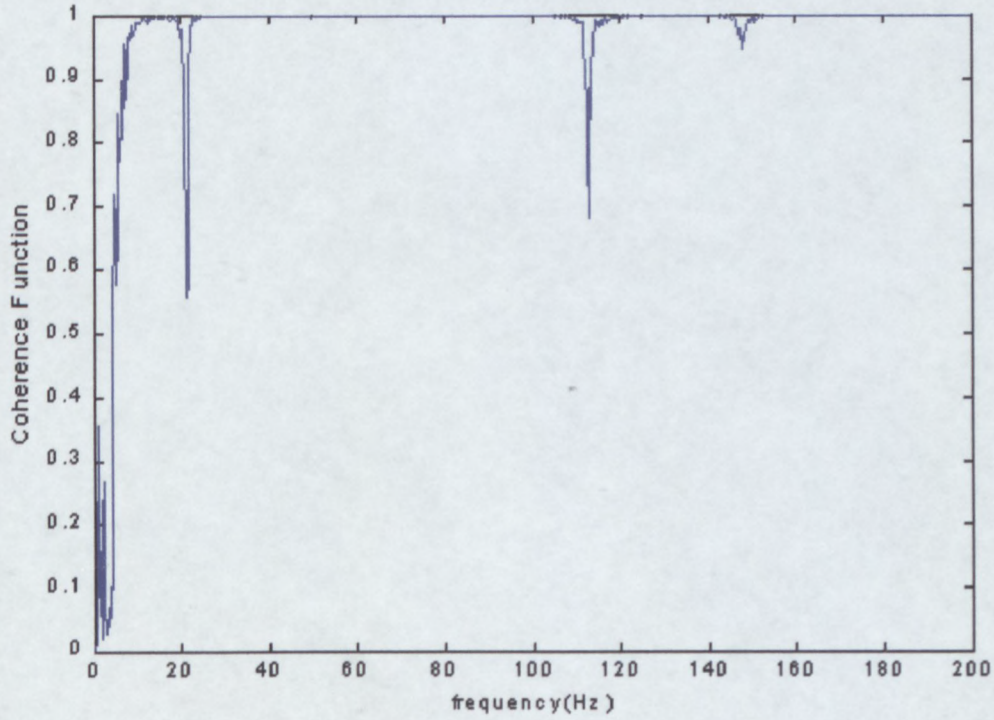

Figure 2.1-7: Coherence Data of Transfer Function

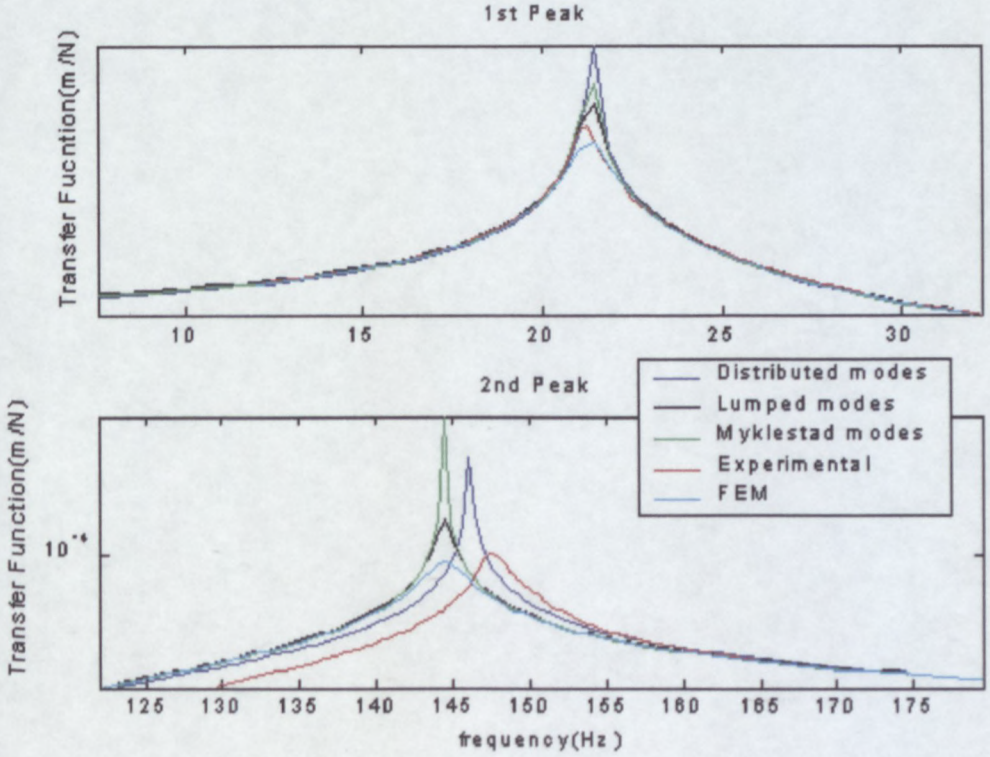

Figure 2.1-8: Predicted and Measured Tip to Tip Resonance Peaks

3 TAIL BOOM VIBRATION ANALYSIS

A basic model of the helicopter tail boom is manufactured to provide a test structure for the analysis of tail boom vibrations. The Finite Element modelling method is used to develop a theoretical model of the basic tail boom structure. The theoretical model is tested to ensure correlation with experimental measurements and is used to verify the effectiveness of the vibration suppression system design.

3.1 BASIC TAIL BOOM STRUCTURE

Helicopter vibrations, caused by the main rotor assembly, are usually analysed by assuming the response of the fuselage to react in a similar manner to that of a 'free-free' beam, as shown in Figure 3.1-1 (a) taken from Tse, Morse & Hinkle[3].

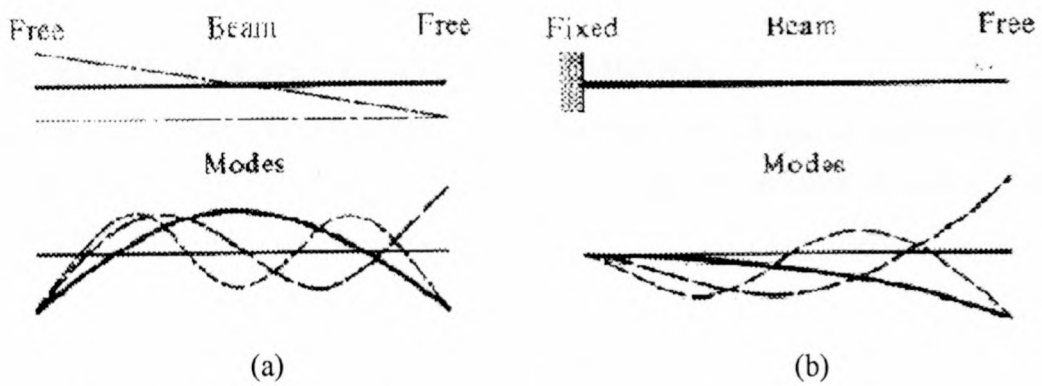

Figure 3.1-1: Modes Shapes of Beam Structures for Different Boundary Conditions

Analysing the effect of tail rotor vibrations requires investigation into the structure of the helicopter. The main rotor assembly and cockpit area are of considerably greater mass when compared with the mass of the tail rotor assembly. Thus the helicopter structure can be modelled to first approximation as a large point mass (the main rotor assembly and cockpit) connected by the relatively slender tail boom to a small point mass (the tail rotor assembly). Because of this significant difference in mass, the tail boom is, for the purposes of this thesis, satisfactorily modelled as a beam structure which is rigidly clamped at the large cockpit mass and has an end mass equal to that of the tail rotor assembly. The mode shapes of a cantilever beam are depicted in Figure 3.1-1(b).

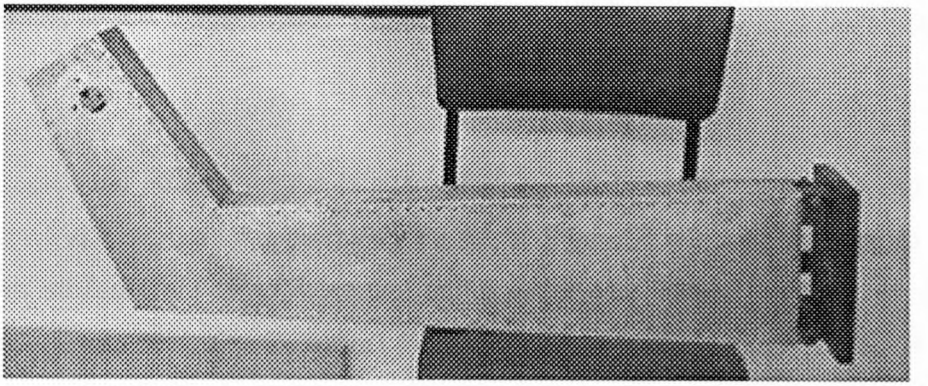

Figure 3.1-2: Basic Tail Boom Test Structure

Figure 3.1-2 illustrates the basic tail boom test structure. The design includes a tapering boom and tail section, strengtheners, stiffeners and a riveted thin outer skin. The complex elliptical form of the actual structure was however replaced by a simple rectangular profile for ease of manufacture.

3.2 FINITE ELEMENT TAIL BOOM MODEL

The finite element model of the tail boom test structure is developed in Msc/NASTRAN for windows (a commercial FE software Package), using the technical drawings of the design, and is illustrated in Figure 3.2-1.

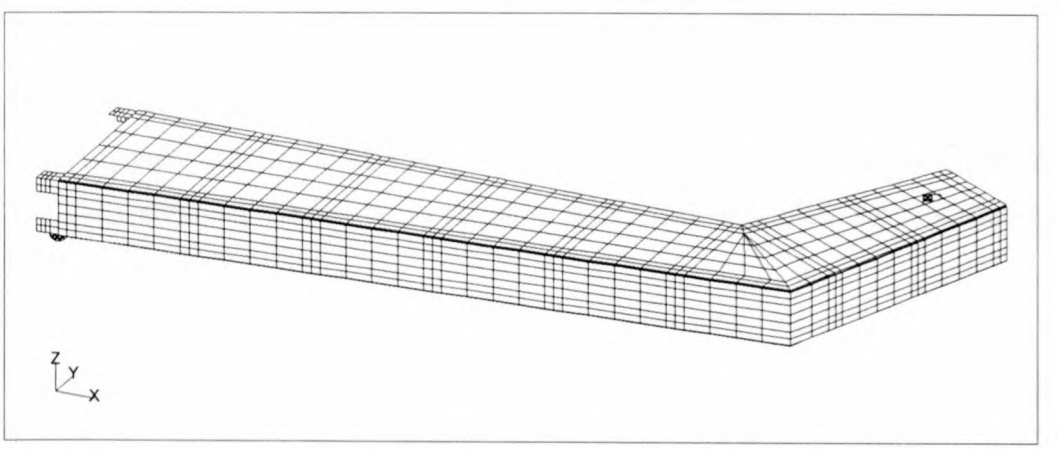

Figure 3.2-1: Finite Element Tail Boom Model

The strengtheners, stiffeners, hub fixture and skin that together form the entire structure of the designed boom, are modelled using SHELL-elements from the NASTRAN element library. SHELL-elements are primarily used because most of the structure has high ratios of in-plane to thickness dimensions. The riveted skin is modelled at the required attachment points using RIGID-elements.

The hub mass and other specific components (e.g. accelerometers) are modelled as concentrated masses, using MASS- elements, and fixed rigidly at the applicable points on the structure.

The designed tail boom structure is attached to a solid fixture using a mounting plate. The fixture is a very thick steel plate, shown in Figure B.1-2, and assumed to be of sufficient stiffness so as to have no influence on the natural frequencies of the experimental structure. The mild steel mounting plate is modelled in NASTRAN using SHELL-elements for the back plate and SOLID-elements for the mounting blocks (due to their relative thickness), as illustrated by Figure 3.2-2.

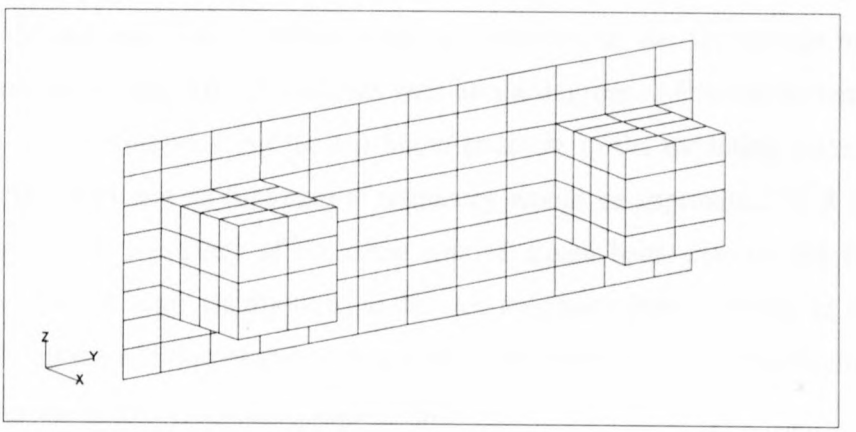

Figure 3.2-2: Finite Element Mounting Plate

From the assumption made about the rigidity of the solid fixture, the nodes at which the mounting plate is bolted to the steel fixture are constrained in all six degrees of freedom. The bolts attaching the tail boom structure to the mounting plate are modelled using RIGID-elements.

Elastic isotropic materials are used in the FE model for both the aluminium structures and the mild steel boom fixture. Aluminium has a Young's modulus of 69 GN/m^2, (Poisson's ratio of 0.25) and mild steel, a Young's modulus 206 GN/m^2, (Poisson's ratio of 0.3). The dynamic tail boom FE model relies on the accuracy of the FE modelling of the tail boom design as well as the mounting plate and clamping conditions of the fixture on which the test structure is mounted.

3.2.1 Requirements for Finite Element Model Correlation

The finite element model is assumed approved to represent the actual test hardware dynamic behaviour if the following correlation requirements for bending, axial and torsional modes (measured modes <100 Hz) are met.

- < 5% frequency correlation to the experimentally measured modes' frequency
- mode shapes of the analytical and experimental modes show acceptable agreement

3.2.2 Verifying Clamping Conditions

Modelling the mass tests the rigidity of the steel fixture and mounting plate combination and moments of inertia of the FE tail boom as one grid point at its centre of gravity, using the MASS-element. The MASS-element is connected to the appropriate nodes on the mounting plate using RIGID-elements with all six degrees of freedom constrained in the regions of the bolts securing the tail boom structure to the mounting plate. The set-up was designed so that its first natural frequency would be approximately 3 times higher then the natural frequency of the same type of model behaviour for the complete FE model of the tail boom rigidly fixed at the mounting plate bolting nodes. In this way it is ensured that the addition of the mounting plate FE model to the FE tail boom model will not lower the natural frequencies significantly.

Figures 3.2-3 and 3.2-4 show the first and third mode shapes of the finite element model of the mounting and single point mass and inertia of the tail boom, respectively. These mode shapes correspond to the lateral bending mode shape and the first local mode shape of the mounting plate. From Table 3.2-1, the first natural frequency of the set-up is calculated as 215.3 Hz which is more then 3 times higher then the design mode (63.1 Hz) of the rigidly clamped tail boom FE model, as is desired to ensure rigidity. The addition of the mounting plate model to the tail boom model, however, lowers the first mode (vertical bending mode) by 5 Hz and the third mode (torsional mode) by 6.8 Hz. The mounting plate has a definite effect on the modes of the tail boom and the Finite Element Model of the mounting plate must be tested to ensure its accuracy.

3.2.3 Verifying FE Mounting Plate Model

To verify the finite element mounting plate model, a hollow square sectioned beam (30 mm x 30 mm x 3 mm and 0.5 m long), is attached to the mounting plate and bolted to the fixture. The beam is modelled and analysed using the FE approach as described in Section 2.1.4. The fixture between the mounting plate and the beam is assumed rigid for the analysis. The accuracy of the mounting plate FE model and effectiveness of the bolted clamping conditions is verified by checking correspondence between its first natural frequency and experimental measurements. A bandwidth of 2000 Hz., with a sampling window of 2048 points is selected for the verification test. The excitation range of 0 to 2000 Hz is used, corresponding to the acquisition frequency range.

Table 3.2-2 compares the natural frequencies of the FE mounting-beam and FE mounting plate set-up with experimental measurements. The first calculated mode corresponds to the first bending mode of the beam. The first mode differs by 11.1Hz, a correlation of just over 5%. Comparing the results against the correlation requirements for the finite element model, it is assumed that, at the high resonance frequencies (>150Hz) of the mode, the correlation is accurate and hence the accuracy of the Finite Element mounting plate is acceptable.

3.2.4 Verifying FE Tail Boom

Experimental transfer functions were measured at 40 points along the outer edges and on the upper and lower surfaces of the tail boom test structure, relative to a random force excitation signal applied at the hub position of the tail boom. The mounted test structure and accelerometer/shake set-up is shown in Appendix B. A bandwidth of 500 Hz, with a sampling window of 2048 points is used. The excitation range of 0 to 500 Hz is used, corresponding to the acquisition frequency range. The transfer functions yield sufficient data to determine relatively accurately the mode shapes, natural frequencies and damping ratios of the structure for comparison which the numerical results of the FE model.

The finite element analysis approach uses a harmonic response technique, based on the modal superposition method to calculate the transfer functions of the FE tail boom model in NASTRAN. The damping ratios for the first two modes are calculated from the experimental transfer functions of the tail boom as:

$\zeta_1 = 0.0271$

$\zeta_3 = 0.0252$

From Table 3.2-1, the lateral bending mode differs by 2.7 Hz, a correlation factor of 4.7% and the torsional mode by 38.1 Hz, a correlation factor of 17.3%. The accuracy of the FE model w.r.t the 2nd natural frequency or vertical bending mode is not considered. This is because, for the purposes of the thesis, the suppression system designed in section reduces the effects of the lateral vibrations of the tail boom resulting form an excitation force in-line with the thrust of the tail rotor. The lateral motion of the boom must be modelled accurately and therefore only the out-of-vertical mode shapes are considered. Figures 3.2-5 and 3.2-6 show the comparative numerical and experimental 1st and 3rd mode shapes, respectively. The comparative transfer functions are given in Figure 3.2-7 with the coherence data, Figure 3.4-8, illustrating the accuracy of the experimental transfer function measurements.

From the results, the correlation of the mode shapes and natural frequencies all fall within the required specification and the Finite Element Model of the entire tail boom structure is therefore assumed to accurately predict the response of the designed tail boom structure. The natural frequencies of the out-of-vertical modes of the experimental test structure are lower. This is expected because of the non-linearity of the surface contacts, which have stiffness in only one direction whereas the FE model is conservative and accounts for stiffness in both directions, resulting in the higher frequencies.

Natural Frequencies (Hz)	Tail Boom Structure rigidly Clamped	Point mass and inertia attached to Mounting Plate	FE tail Boom Structure attached to Mounting Plate	Experimental Tail Boom
1st	63.1	215.4	58.1	55.4
2nd	141.6	500.9	125.1	--------
3rd	246.9	3260	240.1	202.00

Table 3.2-1: Natural Frequencies of FE models

Natural Frequencies	FE Mounting Beam and Mounting Plate Set-up (Hz)	Experimental Results (Hz)	Correlation (%)	Mode Shape
1st	201.4	190.3	5.7	Horizontal Bending Mode

Table 3.2-2: FE Mounting-beam and Experimental Natural Frequencies

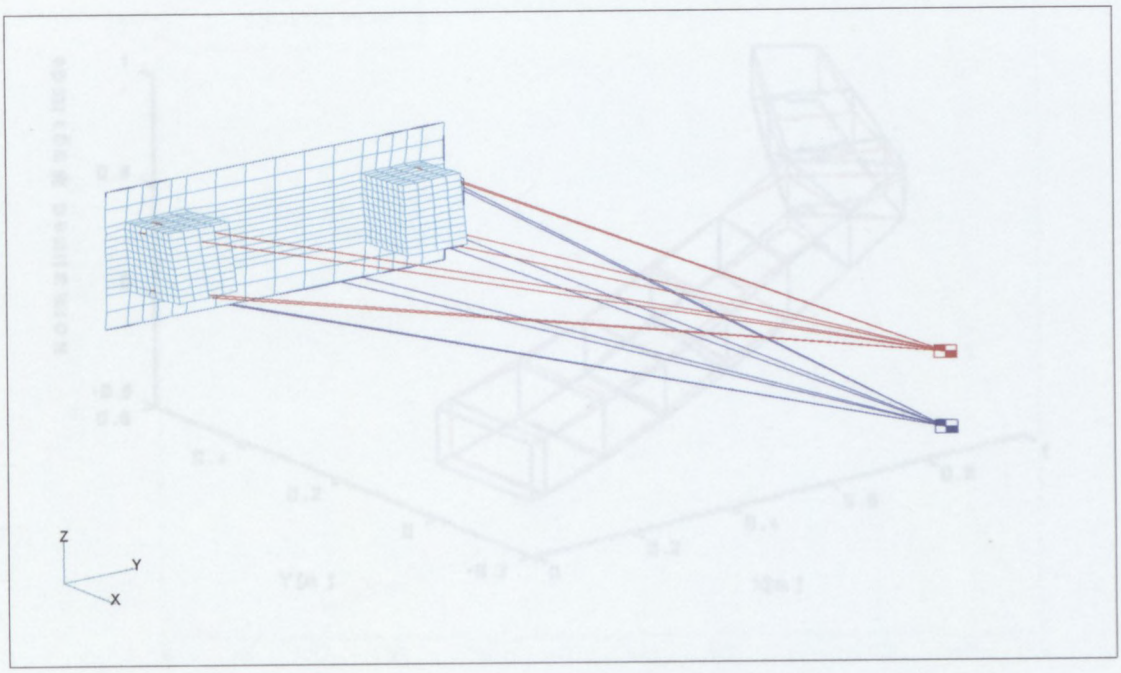

Figure 3.2-3: FE model of Mounting Plate showing First Calculated Mode

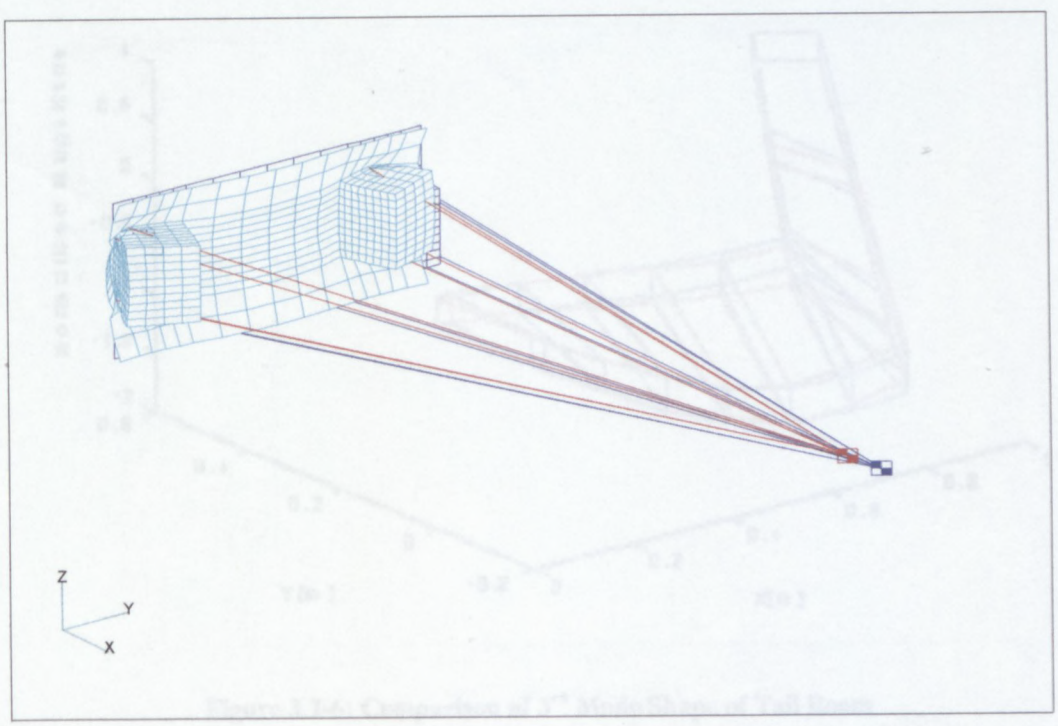

Figure 3.2-4: FE model of Mounting plate showing Third calculated mode

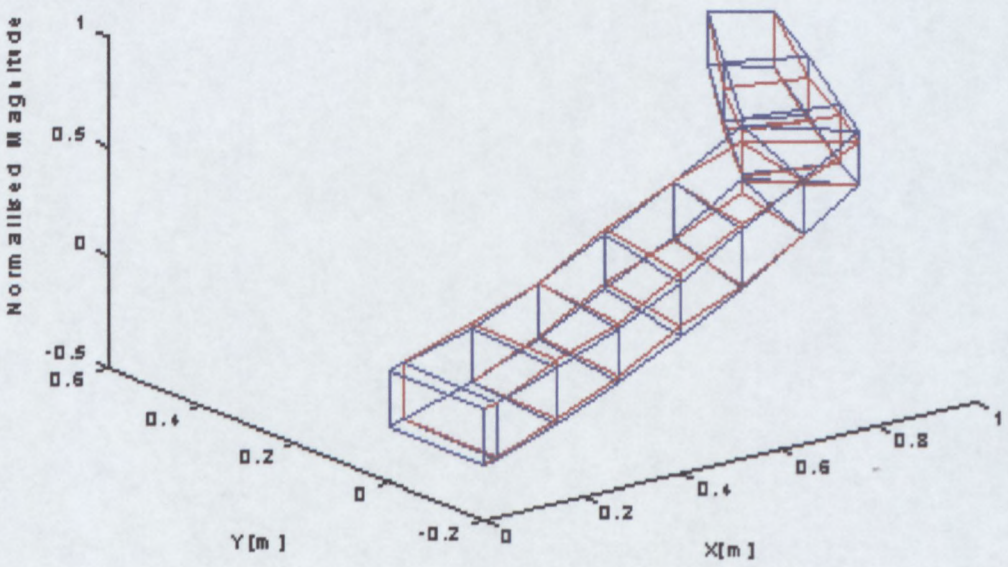

Figure 3.2-5: Comparison of 1st Mode Shape of Tail Boom

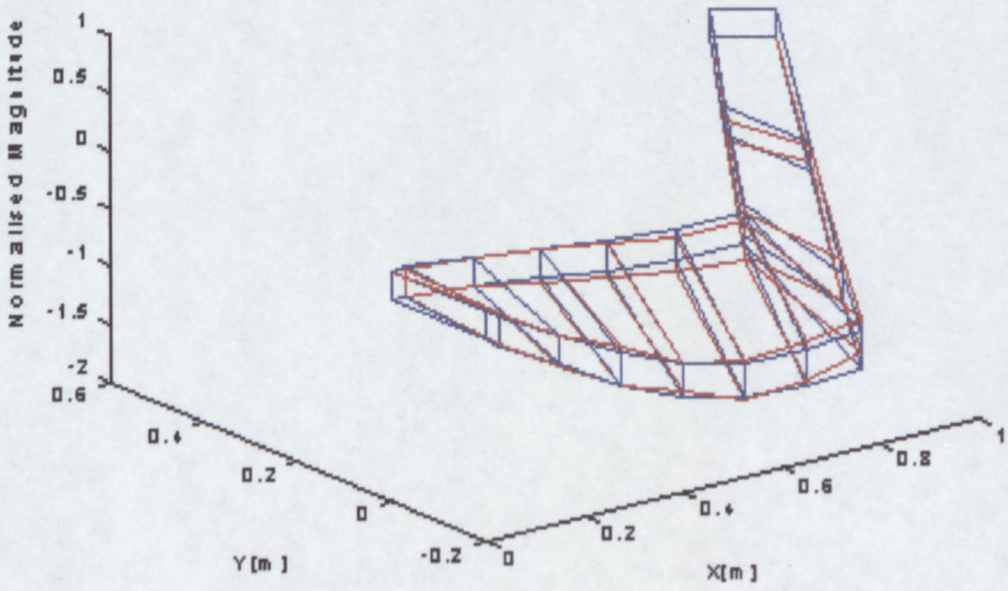

Figure 3.2-6: Comparison of 3rd Mode Shape of Tail Boom

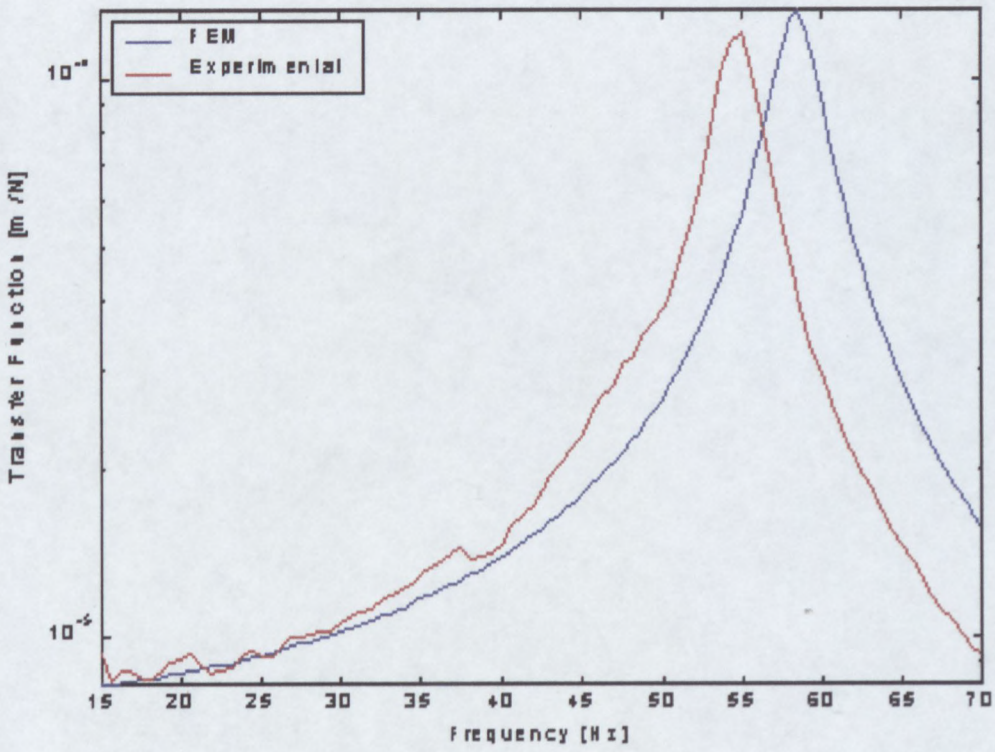

Figure 3.2-7: Predicted and Measured Transfer Function at Hub

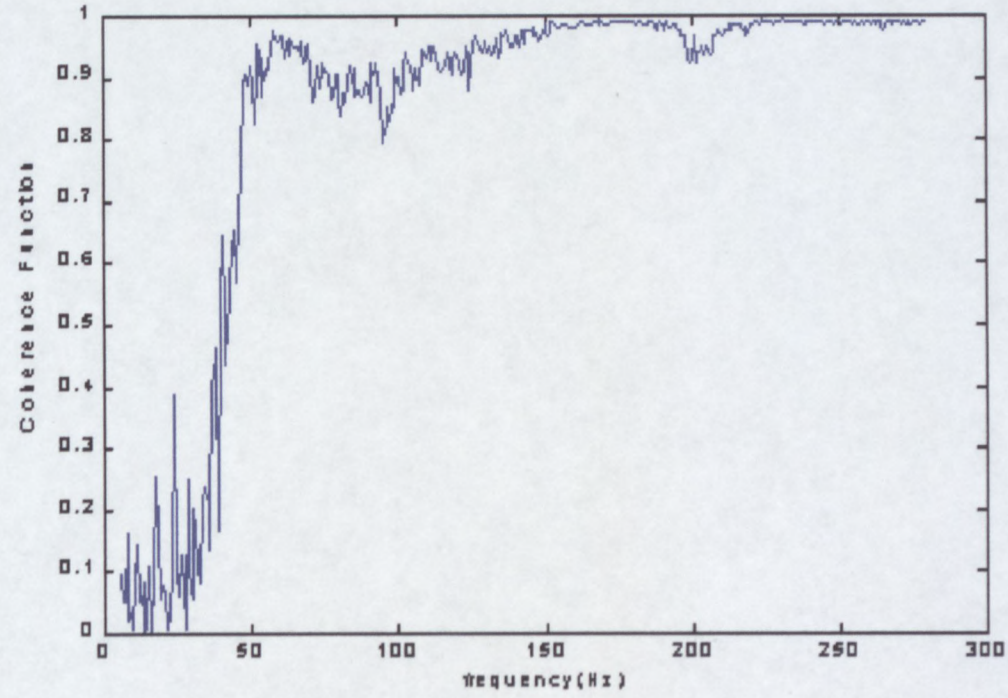

Figure 3.2-8: Coherence Data of Transfer Function

4 TAIL BOOM VIBRATION SUPPRESSION

A vibration suppression system is designed to reduce the resonance peaks at the two dominant frequencies caused by the lateral dynamic force, acting in-plane with the thrust of the tail rotor. The dominant frequencies of the lateral excitation force are estimated using a simplified tail rotor dynamic model and the theoretical results are compared with actual vibration data to determine the accuracy of the model. The designed suppression system is applied to the Finite Element tail boom model and the results are evaluated.

4.1 TAIL ROTOR DYNAMIC ANALYSIS

The dynamic model is restricted for the forward flight and hover regimes of the helicopter, which are assumed prevalent during most flight patterns. The dynamic analysis does not include an investigation of interference effects of the tail boom and ignores external influences such as rotor wake, shear winds, etc. These helicopter main rotor/ tail rotor interactions are investigated by Yin & Ahmed[19] and Basset[20], who produce models of the dynamic inflow of main rotor and tail rotor components.

4.1.1 Tail Rotor Properties

The dynamic theory, presented by Bramwell[11] and Gessow & Myers[12], is based on the main rotor of the helicopter, but can be simplified to reliably predict the behaviour of the tail rotor. The tail rotor differs from the main rotor in many respects that must be accounted for during the dynamic analysis. These include:

- The tail rotor has no cyclic pitch control, but uses a collective pitch system to control the thrust magnitude.
- The tail rotor, for the purpose of this thesis, contains only a flapping hinge.
- The tail rotor acts in a vertical plane and includes no swash plate; thus the no-feathering axis coincides with the hub-plane.

It is assumed that the flapping hinge is situated at an offset from the axis of rotation and the blade flaps through an angle of β . Then, if A, B, C are the moments of inertia around the spanwise, chordwise and normal blade axes respectively, and the blade is modelled as a lamina, it follows that $C = A + B$.

4.1.2 Orthogonal Reference Axes

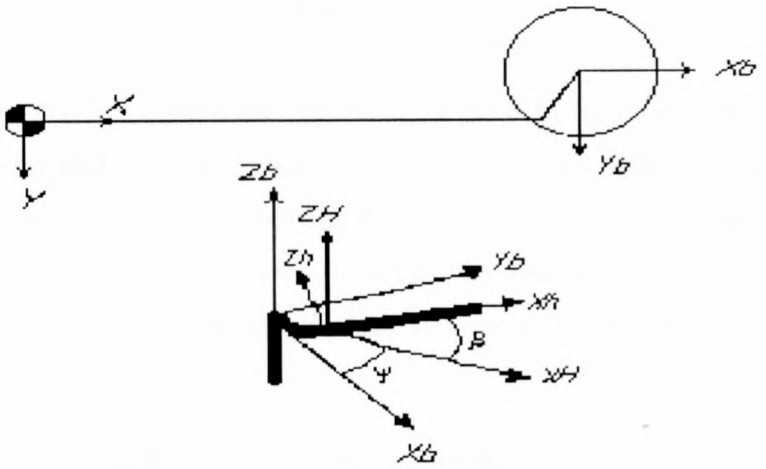

Figure 4.1-1: Axis Definition

Figure 4.1-1 illustrates the axis definitions used in the tail rotor dynamic study. A body axis frame, which is assumed inertial for analysis purposes, is orientated at the CG of the helicopter. The X-axis pointing towards the rear of the helicopter, Y-axis vertically down and Z-axis completing the inertial frame. Axis system b is defined at the hub of the tail rotor with the same orientation as the body axis system.

The hub fixed axis system H is defined as relative to the b-basis and rotated through the azimuth angle Ψ, as xH, yH, zH.

For blade flapping, axis system h, is defined parallel to the principal axis with its origin at the hinge, where the xh-axis points outwards along blade span, yh-axis points chordwise towards the leading edge and the zh axis completing the right - hand set.

4.1.3 Steady State Excitation Forces

The reactions at the hinge of the blade, orientated relative to the b basis, are assumed periodic and are expressed in the form of a Fourier series. The total Z-force, applicable for the design of the suppression system, is therefore defined by Bramwell[11], pg. 347, as

$$Z = -b\left[U_o + \sum_{n=1}^{\infty}\left(U_{nb}\cos(nb\psi) + V_{nb}\sin(nb\psi)\right)\right] \qquad \text{[4.1.3-1]}$$

U_{nb}, V_{nb} are the amplitudes of the Fourier series

The total force is dependent on the number of blades of the tail rotor and the magnitudes of the periodic reaction forces at the hinge. The magnitudes of the forces are based on the properties of the rotor blades and tail rotor.

Because the suppression system is designed only to counteract the dominant frequencies of excitation caused by the rotor blades, the magnitudes of the forces are not important and the properties are selected arbitrarily.

To test the assumption that the reactions are periodic, as defined by equation 4.1.3-1, a dynamic analysis is performed on the tail rotor of the helicopter. Assuming all blades are identical, the reaction forces and their relationships with the torque can be derived from the dynamic analysis of a single blade. The total forces are obtained by summing the effects of each of these single blade reaction forces by the number of tail rotor blades present.

4.1.4 Single Blade Dynamic Analysis

The dynamic analysis is formulated for steady forward flight and hover. The components R_x, R_y, R_z of the reactions acting at the hinge caused by a single blade are determined using Newton's Law. The equations of the dynamic motion are therefore defined as:

$$\bar{f}_b + \bar{R} = m_b \bar{a}_{g/CG} \qquad \text{[4.1.4-1]}$$

The definitions of the acceleration vector $a^b{}_{g/CG}$ and aerodynamic forces vector f_b^b are resolved into the non-rotating b-basis, relating to the hub position of the tail rotor. The acceleration components are derived from the definitions of particle acceleration of rotating bodies using position vectors and angular rotation definitions defined according to their basis axis systems or relative to a desired basis system. The aerodynamic elementary forces on individual blades are derived from the analysis of the blade lift and drag components.

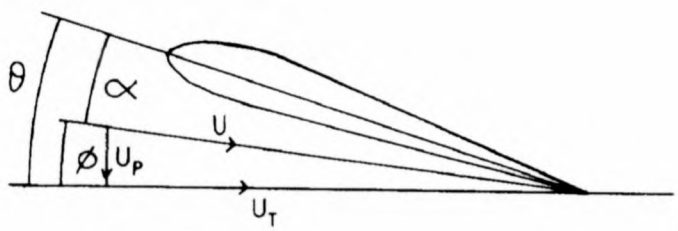

Figure 4.1-2: Velocity Components of a Single Blade

From figure 4.1-2, taken from Bramwell[11], the lift and drag components are dependent on the relative wind velocity of the blade. For the tail rotor, which is upright in the flow during forward flight, ignoring shear winds and other external influences, $\bar{V}_\infty = V_{ff}\bar{e}_X^b$ and the relative wind components are calculated as:

$$U_T = \Omega R_b (x + \mu \sin \Psi) \qquad [4.1.4\text{-}2]$$

$$U_p = \Omega R_b (-x\dot{\beta} - \lambda_i - \beta\mu \cos \Psi) \qquad [4.1.4\text{-}3]$$

The advance ratio μ, inflow ratio λ_i and normalised position x along the blade span are defined by:

$$\mu = V_{ff}/\Omega R \qquad [4.1.4\text{-}4]$$

$$\lambda_i = v_i/\Omega R \qquad [4.1.4\text{-}5]$$

$$x = r_b/R_b \qquad [4.1.4\text{-}6]$$

The velocity equations are converted from the time dependent flap angle β into an azimuth angle dependent variable using $\partial\beta/\partial t = \Omega\partial\beta/\partial\psi$. Taken from Bramwell[11], pg. 145-150, the elementary force and torque equations for an individual blade are given as:

$$dT = \tfrac{1}{2} a\rho\left[\theta_o U_T^{\,2} + U_P U_T\right] c R_b dx_b \qquad [4.1.4\text{-}7]$$

$$\begin{aligned} dH &= dH_o + dH_i \\ dH_o &= \tfrac{1}{2}\rho U_T^{\,2}\delta c \sin\psi R_b dx_b \\ dH_i &= -\tfrac{1}{2}\rho a\left[\left(\theta_o U_T^{\,2} + U_P U_T\right)\beta\cos\psi + \left(\theta_o U_P U_T + U_P^{\,2}\right)\sin\psi\right] c R_b dx_b \end{aligned} \qquad [4.1.4\text{-}8]$$

$$dQ = \tfrac{1}{2}\rho U_T^{\,2}\delta c R_b^{\,2} x_b dx_b - \tfrac{1}{2}\rho U_T^{\,2} a\varphi\alpha\phi c R_b^{\,2} x_b dx_b \qquad [4.1.4\text{-}9]$$

These elementary aerodynamic forces are integrated over the length of the blade to obtain expressions for the instantaneous forces and torque associated with individual blades in terms of azimuth angle. The blade forces and torque depend on the flapping motion, flapping velocity and flapping acceleration of the COG of the blade, thus a solution of the flapping motion of the blade must be found.

4.1.4.1 Flapping Equation

An expression for the flapping equation of the blade is derived from the investigation of rigid body angular momentum around the flapping hinge, using an extended Euler equation. Because, the flapping moment is zero at the hinge, an expression defining the flapping equation is derived, which is dependent on the aerodynamic flapping moment at the hinge. The resulting equation is calculated relative to the H basis as:

$$\ddot{\beta} + (1+\varepsilon)\beta = M_A/\Omega^2 B \qquad [4.1.4\text{-}10]$$

$$\varepsilon = M_b r_{cg} e r / B$$

The aerodynamic flapping moment M_A is calculated, w.r.t the H basis as:

$$M_A = \int_0^1 R_b x_b \tfrac{1}{2} \rho a c R_b \left(\theta_o U_T^{\,2} + U_P U_T\right) dx_b \qquad \text{[4.1.4-11]}$$

The steady state flapping motion is assumed to be stable and a Fourier series describe the solution.

$$\beta(\psi) = \beta_0 + \sum_{n=1}^{\infty} \left(A_{\beta n} \cos(n\psi) + B_{\beta n} \sin(n\psi)\right) \qquad \text{[4.1.4-12]}$$

Substituting this series as well as the series derivatives into aerodynamic flapping equation, the coefficients of the terms $\sin(\psi), \cos(\psi)$..... on the left- and right- hand side of the equation are equated. From the assumptions of Gessow and Myers [12], pg. 199, the higher harmonics of the flapping equation can be ignored. Therefore we consider only the constant term and the two first-harmonic terms. The steady state flapping coefficients are calculated for the tail rotor in forward flight as:

$$\beta_0 = \tfrac{\gamma}{8}[\theta(1+\mu^2) - \tfrac{4}{3}\lambda_i] \qquad \text{[4.1.4-13]}$$

$$A_{\beta_1} = -\mu(\tfrac{8}{3}\theta - 2\lambda_i)/(1 - \tfrac{1}{2}\mu^2) \qquad \text{[4.1.4-14]}$$

$$B_{\beta_1} = -\tfrac{4}{3}\beta_0 \mu / (1 + \tfrac{1}{2}\mu^2) \qquad \text{[4.1.4-15]}$$

which correspond accurately with the steady state results formulated in Bramwell[11], pg. 155.

4.1.5 Induced Velocity

Under the assumptions of Gessow & Myers [12], pg. 199,the induced velocity field along the blade is assumed uniformly distributed along the blades. As formulated by Bramwell[11], pg. 77, the actuator-disc theory is used to define the induced velocity in hover, whereas, the Glauert formula is used during forward flight. Glauert's formula is given in Bramwell[11], pg. 124, as:

$$v_i = T / 2\rho A \tilde{V} \qquad \text{[4.1.5-1]}$$

$$\tilde{V} = \sqrt{V_\infty^{\,2} + v_i^{\,2}}$$

A is the rotor area

4.1.6 Trim analysis

The tail rotor is a small diameter rotary wing with the function of balancing the main rotor torque and providing yaw control. The trim analysis is used to define the exact collective pitch angle of the tail rotor to ensure balancing of the main rotor torque. Ignoring the effect of a tail plane and assuming that the fuselage pitching moment is zero, the trim conditions of the main rotor are calculated for a forward flight velocity ranging from 0 to 45m/s using equations derived by Bramwell[11]. Assuming a small rotor-disc incidence, Bramwell's formulations lead to the derivation of the governing equation in a non-dimensional form, which calculates the main rotor incidence α_D as:

$$\alpha_D = -\left(\tfrac{1}{2}\hat{V}^2 d_o + h_{cD}\right)\Big/ t_{cD} \qquad \text{[4.1.6-1]}$$

$$\hat{V} = V_{ff}/\Omega R,$$

$d_o = D_o/sA$ where D_o is the so-called equivalent flat-plate area

$h_{cD} = \tfrac{1}{4}\mu\delta$ as a first approximation

$t_{cD} = W_c$ which is due to the small rotor-disc incidence

The main rotor inflow ratio for the trim conditions λ_D is approximated using

$$\lambda_D = (\mu\alpha)_D - \lambda_i \qquad \text{[4.1.6-2]}$$

where the induced inflow ratio λ_i is calculated using the induced velocity component v_i of the rotor for the specific flight regime, as defined in Section 4.1.5. According to Bramwell[11], pg.166, the results are only a first approximation but are sufficiently accurate to be used in further calculations. To ensure the helicopter is in a trimmed condition during hover or forward flight, the pitch angle of the tail rotor must be calculated to ensure that the tail rotor thrust cancels the effect of the main rotor torque.

The main rotor torque coefficient can be calculated using the disc axis equation defined in Bramwell[11], pg. 157, as

$$q_c = \delta\left(1 + 3\mu^2\right)/8 - \lambda_D t_{cD} - \mu h_{cD} \qquad \text{[4.1.6-3]}$$

Assuming the tail rotor thrust moment is the only moment balancing the main rotor torque, the tail rotor thrust is calculated from:

$$T_t = Q/l_t R_t \qquad \text{[4.1.6-4]}$$

$$Q = q_c \rho s A \Omega^2 R^3$$

Following the assumptions and formulations in Bramwell[11], the collective pitch angle of the tail rotor is calculated using the equation:

$$\theta_{0t} = \frac{3}{2(1+3\mu^2/2)}\left(\frac{4}{a}t_{ct} - \lambda_{it}\right) \qquad \text{[4.1.6-5]}$$

$$t_{ct} = T_t / \rho s_t A_t (\Omega R)_t^2$$

$$\lambda_{it} = \sqrt{s_t t_{ct}/2} \text{ in hovering flight}$$

$$\lambda_{it} = s_t t_{ct}/2\mu \text{ for } \mu > 0.05$$

The variation in collective pitch angle of the tail rotor w.r.t the forward flight velocity for trim is calculated using the data in Appendix C.1 and is shown in Figure 4.1-3. The helicopter is assumed to have a four bladed main rotor and a two bladed tail rotor.

4.1.7 Steady State Results

Using an appropriate collective pitch angle of the tail rotor in trim and the calculated flapping coefficients, the aerodynamic forces can be derived instantaneously at any azimuth angle of the blades. Incorporating the acceleration components and aerodynamic forces into Equation 4.1.4-1, the reaction forces at the hinge, caused by a single blade can be calculated. The total reaction forces at the hinge are found by summing the influence of each blade of the tail rotor. Simulations are run in MATLAB, using atmospheric properties and helicopter data given in Appendix C.1.

Figure 4.1-4 shows the behaviour of the trimmed Z-force at hover and forward flight speeds of 15, 30 and 45 m/s, associated with the two-bladed tail rotor. As expected, the Z force is at a constant magnitude during hover and is periodic in nature. Comparing the assumed nature of the vibratory forces, defined by Equation 4.1.3-1, the simulation yields only the 2/rev oscillatory term, as shown by the normalised spectral representation of the force at 30m/s forward flight velocity, Figure 4.1-5. The 'loss' of the higher harmonic oscillatory terms in deriving the forces is probably a result of assuming that the higher harmonics of the flapping equation can be ignored.

The relationships between the mean H-force, torque, thrust and steady state flapping coefficients w.r.t forward flight velocity are given in Figure 4.1-6 to 4.1-9 respectively.

4.1.8 Actual Vibration Data Comparisons

Actual vibration data using an existing ROTORTUNE system is obtained from two, 5-bladed tail rotor, SAAF ORYX helicopters in hover and forward flight, and is given in Appendix C.2. The actual data gives velocity spectra only and it is somewhat questionable to compare this data to the excitation force data calculated in the analytical process. The vibration data is, however, used to only validate the calculated Z-force dominant frequencies and indicate any extra frequencies caused during normal operating conditions. For this reason and for lack of other measurements the comparison is assumed acceptable.

The velocity spectrums for hover and forward flight indicate the 5/rev and 10/rev frequencies as is expected from analysis of equation 4.1.3-1 and from the calculation process. The 10/rev magnitude is however shown to be distinctively smaller then the magnitude of vibration velocity caused at the 5/rev frequency. The data additionally indicates a wide spectrum of vibration data in the low frequency region. A significant peak is however viewed at the 1/rev frequencies, which is not described by the dynamic theory. This peak is associated with the rotational speed of the tail rotor. From the evaluation for the actual data, the higher harmonic magnitudes are assumed to be negligible when compared to the vibration effects caused by the 1/rev and 5/rev frequencies. Adapting and simplifying equation 4.1.3-1 to incorporate these findings, the Z-force is defined as:

$$Z = Z_o + Z_1 \sin(\psi) + Z_b \sin(b\psi) \qquad \text{[4.1.8-1]}$$

The magnitudes of the dominant frequencies of the reaction Z-force are not essential to the design of the vibration absorber. For the purposes of this thesis, they are therefore assumed equal and of unit magnitude.

Without sufficient in-flight vibration data, the dynamic results cannot be justified reliably. More significantly, the theory does not incorporate non-ideal components, i.e. loose or worn hinge joints, non-identical blades, blade imbalance etc. It is therefore necessary to provide a more in-depth analysis and study of the dynamic theory to ensure that the dynamic model is effective. For this thesis, however, the results provide first approximations of the actual forces and are assumed to reveal the basic frequency trends reliably.

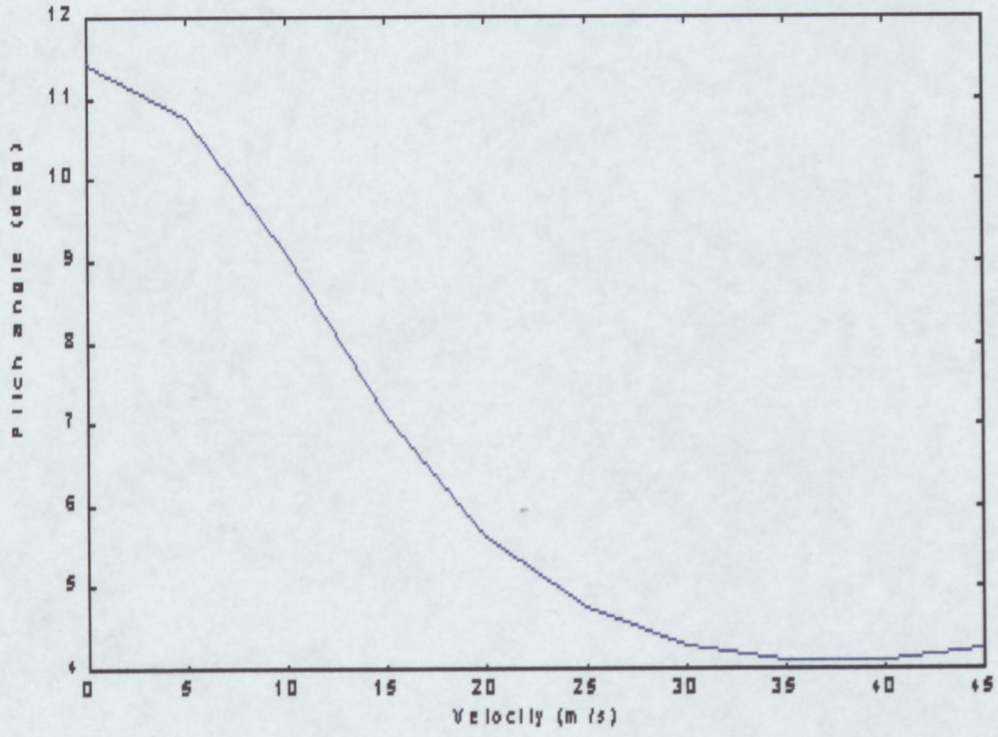

Figure 4.1-3: Tail rotor Collective Pitch in trim

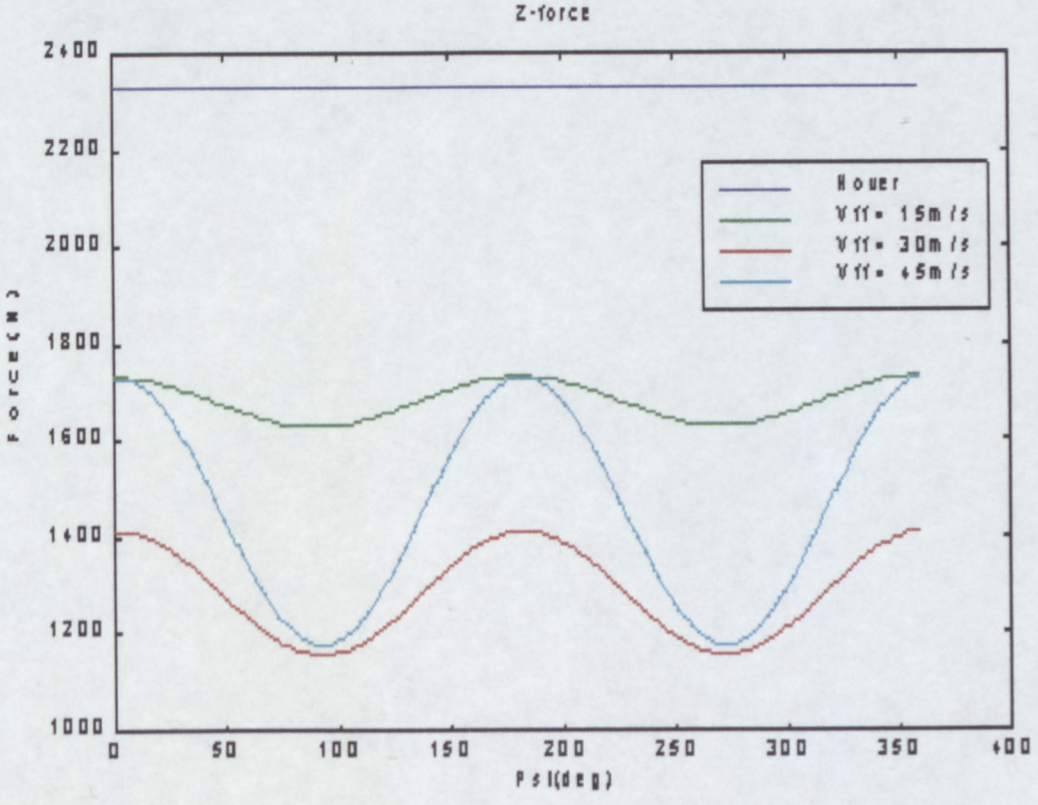

Figure 4.1-4: Tail Rotor Force (Z-direction) in Trim

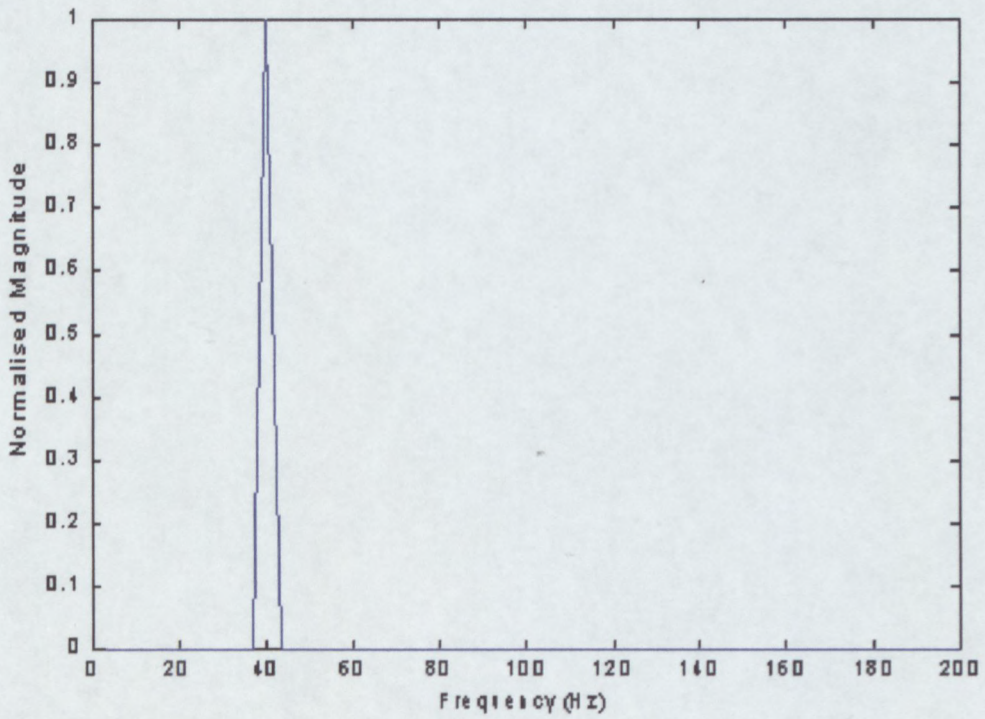

Figure 4.1-5: Normalised Spectral Magnitude of Tail Rotor Z-force in Trim

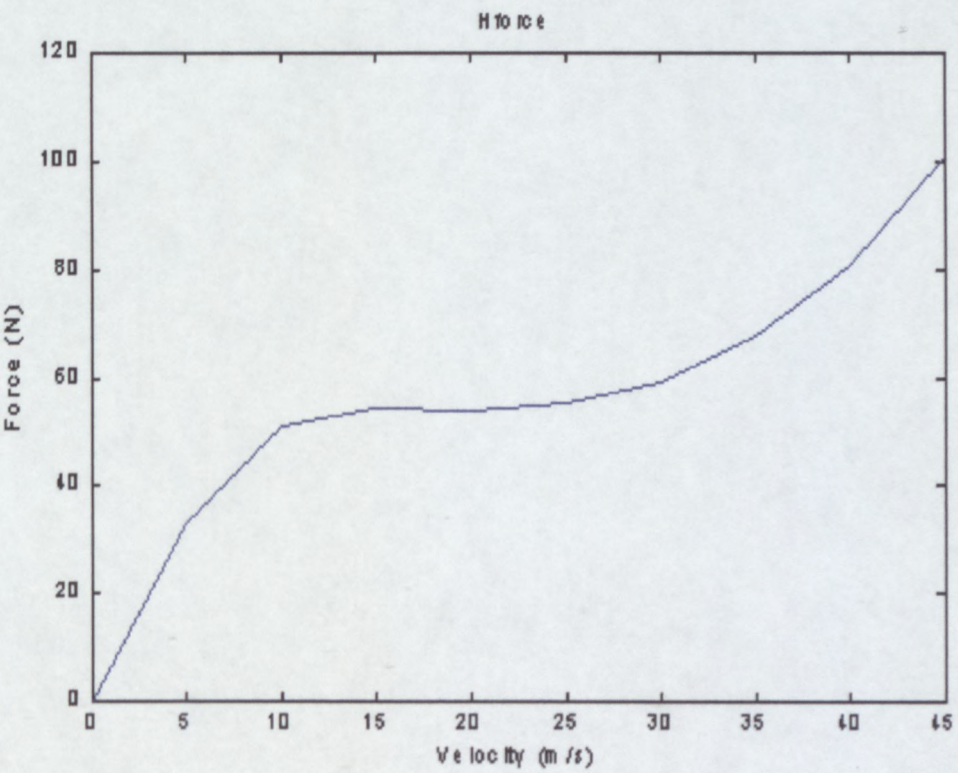

Figure 4.1-6: Tail Rotor H-force in Trim

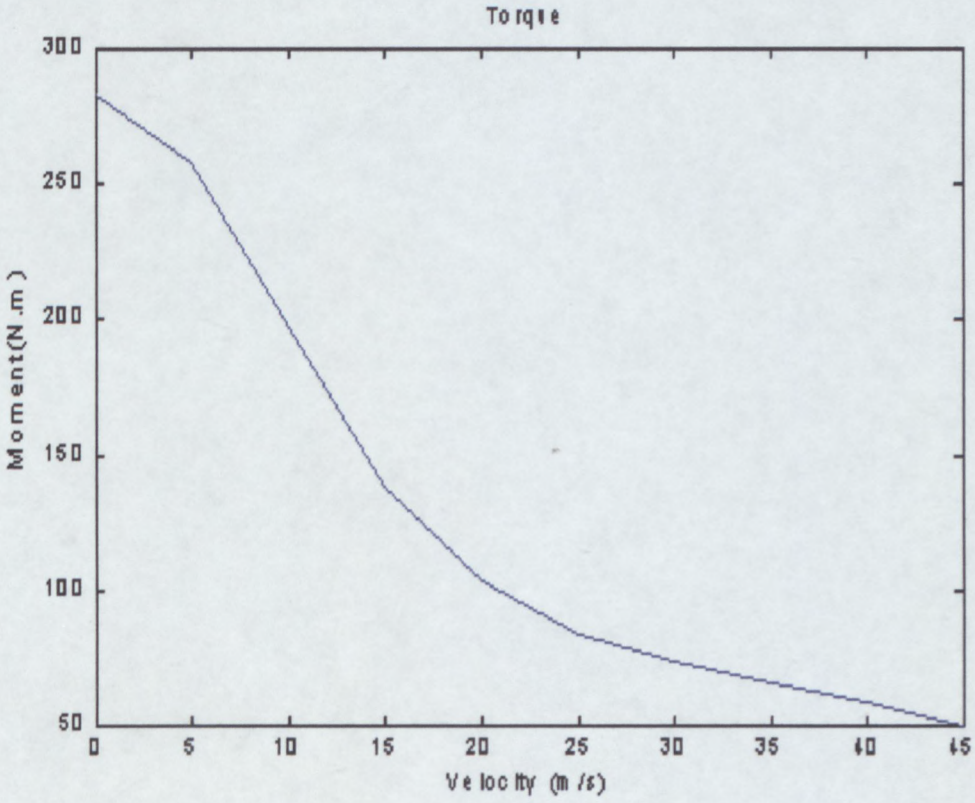

Figure 4.1-7: Tail rotor Torque in Trim

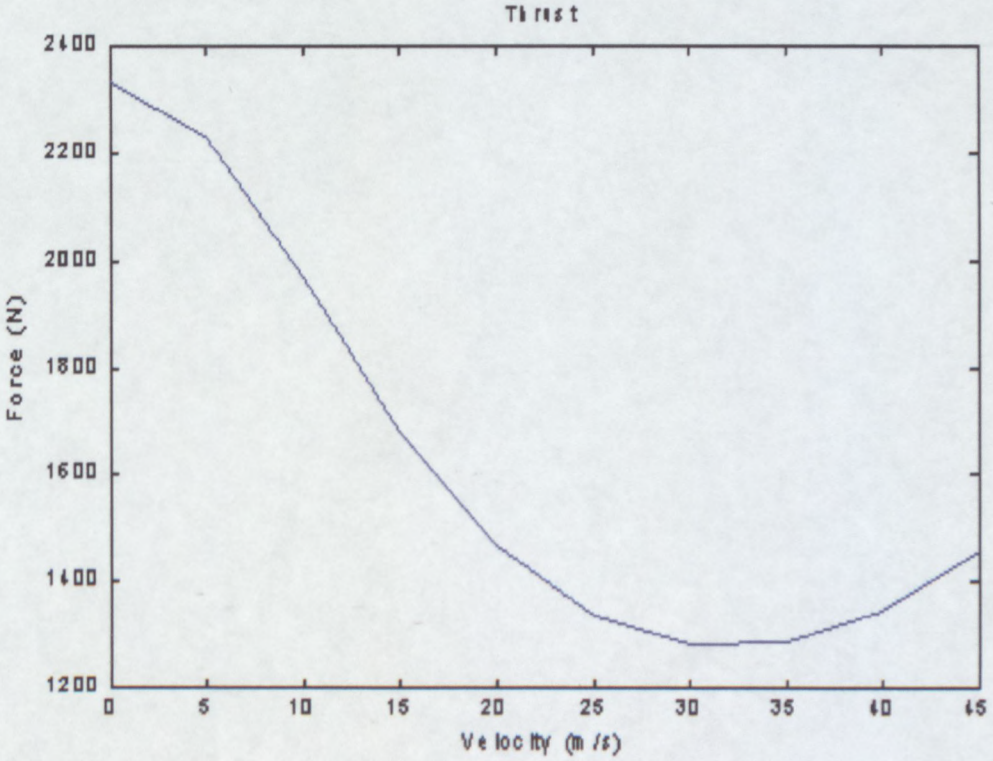

Figure 4.1-8: Tail Rotor Thrust in Trim

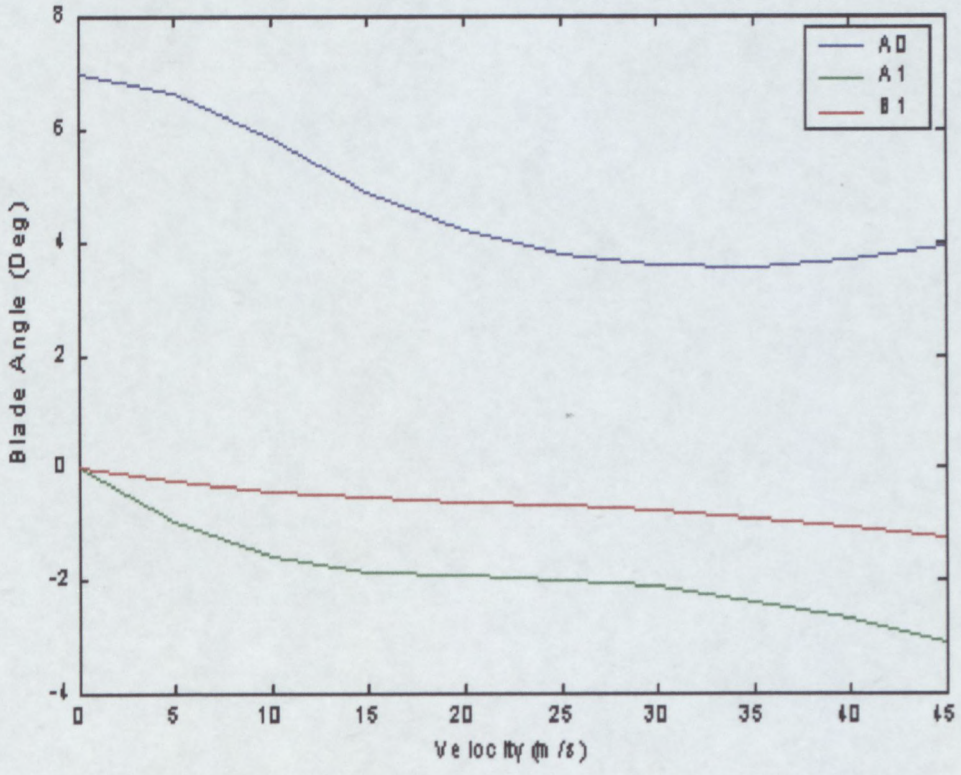

Figure 4.1-9: Tail Rotor Flapping Coefficients in Trim

4.2 VIBRATION SUPPRESSION SYSTEM DESIGN

A theoretical vibration suppression system is designed to reduce the resonance peaks at the two dominant frequencies produced by rotor dynamics of the blades. These are, from the derived Z-force, Equation 4.1.8-1, the effects of the 1/rev and 2/rev excitation frequencies, for a two bladed tail rotor. A design procedure is formulated and tested analytically, using a simple cantilever beam structure. The tested procedure is then applied to the finite element theoretical model of the tail boom and the effectiveness of the suppression system is evaluated.

4.2.1 Design Procedure

The proposed design procedure firstly assumes that a beam structure can be reduced to a single degree of freedom system, which reacts in a similar manner to the complex system response at low frequencies (see Aida et al[15]). Any complex system thus reduces to a single degree of freedom effective mass-damper-spring system. Secondly, the design procedure assumes that dynamic absorbers optimised w.r.t. this effective model will provide sufficient suppression of the vibratory response when applied to the actual complex system.

4.2.2 Absorber Theory

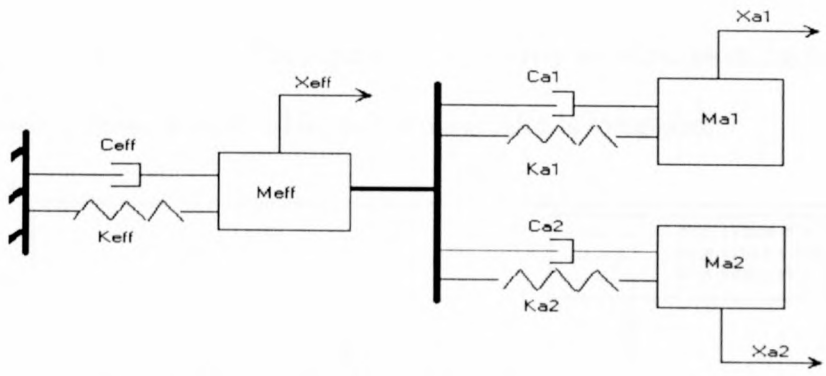

Figure 4.2-1: Simplified Three Degree of Freedom System

For the purposes of this thesis, two absorber mass-damper-spring sub-systems, counteracting the two excitation frequencies of the applied forces are attached to the effective components of the system, as shown in Figure 4.2-1. The equations of motion are derived using the lumped parameter approach and the response of the damped absorber system, is calculated as:

$$X_{eff} = -\frac{1}{\Delta(\omega)}(-m_{a1}\omega_{dr}^2 + ic_{a1}\omega_{dr} + k_{a1})(-m_{a2}\omega_{dr}^2 + ic_{a2}\omega_{dr} + k_{a2})F_{eq} \quad \textbf{[4.2.2-1]}$$

$$X_{a1} = \frac{1}{\Delta(\omega)}(ic_{a1}\omega_{dr} + k_{a1})(-\omega_{dr}^2 m_{a2} + i\omega_{dr}c_{a2} + k_{a2}) \quad \textbf{[4.2.2-2]}$$

$$X_{a2} = \frac{1}{\Delta(\omega)}(ic_{a2}\omega_{dr} + k_2)(-\omega_{dr}^2 m_{a1} + i\omega_{dr}c_{a1} + k_{a1}) \quad \textbf{[4.2.2-3]}$$

$$\Delta(\omega) = \det\left(-\omega_{dr}^2[M] + i\omega_{dr}[C] + [K]\right)$$

The undamped system provides an understanding of the behaviour of a vibration absorber and insight into the design parameters.

4.2.2.1 Design Parameters

The dynamic absorber must be tuned to ensure the amplitude X_{boom} becomes zero. Assuming damping is negligible, this happens when the absorber frequencies of equation 4.2.2-1 equal the excitation frequencies of the applied force. In this case study, the applied force frequencies are arbitrarily selected as 3 Hz and 5 Hz and the stiffness and mass parameters of the absorbers are tuned to these two frequencies.

The mass ratios m_{a1}/m_{eff} and m_{a2}/m_{eff} also have significant effects on the absorber design. As shown in Figure 4.2-2 the mass ratio m_{a1}/m_{eff} is varied from 0.2 to 0.4 while m_{a2}/m_{eff} is held constant. The figure clearly shows an increase in the breadth of the first anti-resonance peak, around 3 Hz, as the mass ratio is increased.

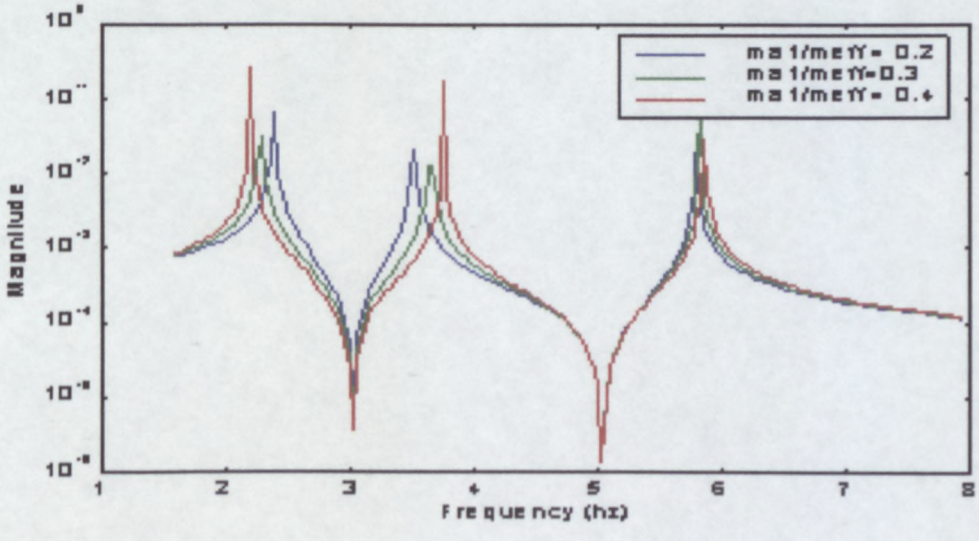

Figure 4.2-2: Influence of mass ratio m_{a1}/m_{eff} on Transfer Function

Figure 4.2-3 depicts a similar trend around the 5 Hz anti resonance peak,, where the mass ratio m_{a2}/m_{eff} is increased while m_{a1}/m_{eff} is held constant.

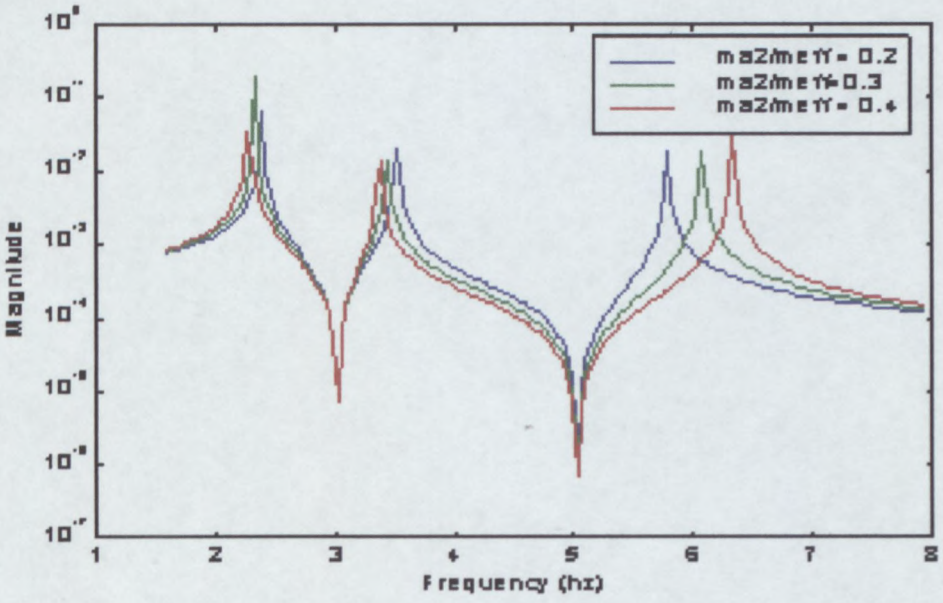

Figure 4.2-3: Influence of mass ratio m_{a2}/m_{eff} on Transfer Function

From this study, it can be concluded that, if the ratios are small, the resonant frequencies are closer together about the resonance frequency of the original system and there is little variation allowed in driving frequency as shown by the 'steep' anti-resonance gradients. As the ratios increase so the anti-resonance gradients decrease, allowing a wider range for variation of the driving frequencies. However, for larger ratios, the mass of the absorber will add considerably to the mass of the system. The design must therefore limit the effect of the added mass caused by the vibration absorber but also ensure an effective variation range of the anti-resonance peaks.

If damping is not negligible, however, the response does not equal zero when the absorbers are tuned to the excitation frequencies because damping reduces the effectiveness of the vibration absorber. The equation is based on specific values associated with the elements of the system where only the effective mass, damping and stiffness of the single degree of freedom boom and the driving frequency are known.

The damping is assumed to have little effect on the influence of the mass ratio design parameter and the effect is assumed similar to that investigated in the undamped system.

4.2.3 Absorber System Optimisation

To ensured optimal design of the absorber system, the response of the boom must be minimised subject to constraints based on the design parameters of the absorber components, described above. The exterior penalty function method presented in Vanderplaats[21], defines the problem statement as follows:

Minimise: F

Subject to $g_j \leq 0 \quad j = 1 \rightarrow m$

$h_k = 0 \quad k = 1 \rightarrow l$

To ensure effective reduction of the dominant resonance peaks, the effective response of the system, Equation 4.2.2-1, must be minimised at the 1/rev and 2/rev frequencies simultaneously. Thus two objective functions F, which are dependant on the two mass ratios, m_{a1}/m_{eff} and m_{a2}/m_{eff} and the two damping coefficients, c_{a1} and c_{a2}, are therefore derived, the first, defined by substituting the 1/rev frequency as the driving frequency of equation 4.2.2-1, and the second, by substituting the 2/rev frequency as the driving frequency of equation 4.2.2-1. The magnitudes of the individual forces require the accurate experimental measurement of the forces, which are unknown. As was assumed in the rotor dynamic study, for the purposes of this thesis, the forces are assumed equal and to have unit magnitude, thus the equations are weighted equally. The optimisation constraints for these objective functions are based on the design parameters as follows:

The mass ratios are limited to a range between 0.2 and 0.25 hence

$$g_1 = m_{a1} - 0.25 m_{eff} \qquad \textbf{[4.2.3-1]}$$

$$g_2 = m_{a2} - 0.25 m_{eff} \qquad \textbf{[4.2.3-2]}$$

$$g_3 = 0.2 m_{eff} - m_{a1} \qquad \textbf{[4.2.3-3]}$$

$$g_4 = 0.2 m_{eff} - m_{a2} \qquad \textbf{[4.2.3-4]}$$

The damping is constrained to be above 0.005 for both absorbers.

$$g_5 = 0.01 m_{a1} \omega_{na1} - c_{a1} \qquad \textbf{[4.2.3-5]}$$

$$g_6 = 0.01 m_{a2} \omega_{na2} - c_{a2} \qquad \textbf{[4.2.3-6]}$$

The optimisation approach is to minimise objective function as unconstrained but provide a penalty to limit the constraint violations. Hence, a pseudo-objective function is derived in the form

$$\Phi = F + pP \qquad [4.2.3\text{-}7]$$

P is the penalty function.

p is the penalty multiplier

The penalty function is defined using the exterior penalty function method, which penalises the objective function only when the constraints are violated.

The penalty function in this case is typically given as

$$P = \sum_{j=1}^{m} \{\max[0, g_j]\}^2 + \sum_{k=1}^{l} \{h_k\}^2 \qquad [4.2.3\text{-}8]$$

showing zero effect to the objective function when constraints are not violated.

The multiplier has a significant effect on the optimisation process. The smaller the value of the multiplier the more efficient the numerical analysis of the resulting Φ function, but at the same time the larger the constraint violations. On the other hand, a large value of p will ensure near satisfaction of all constraints but will create a poorly conditioned optimisation problem form a numerical standpoint. The optimisation method therefore initially minimises the system using a moderate multiplier value. The value is then increased by a factor γ and re minimised, each time using the previous solutions, until the results are satisfactory. The convergence criteria are that the original function F does not change significantly during one unconstrained minimisation and that all constraints are within specified tolerances.

4.2.4 Evaluation of Design Procedure

Modelling the designed vibration suppression system using a Lumped Parameter strategy tests the design procedure and optimisation algorithm. The mass, stiffness and damping matrices are incorporated into the Lumped Parameter model of the cantilever beam already analysed and proven in Section 2.1.1. The effectiveness of this suppression system proves the reliability of the assumptions made in the design procedure, before implementation on the analytical model of the design tail boom.

4.2.4.1 Effective Beam components and Optimised Absorber Parameters

The cantilever test beam is reduced to an effective single degree of freedom system, as assumed by the design procedure. From the analysis of the analytical and experimental results of the beam, the first mode shape is clearly the bending mode of the beam. The effective stiffness is therefore derived using basic beam deflection theory. The effective mass is calculated ensuring correspondence with the beams calculated first natural frequency and the effective damping is calculated using the experimental mass coefficient α and stiffness coefficient β of the beam.

The suppression system is designed to reduce the two dominant frequency effects of the Z-force, derived in the rotor dynamic analysis. The design parameters of the absorber system are optimised using these effective components of the beam, as described in section 4.2.3. After numerous iterations, the convergence criteria were met and the optimal values for the design parameters were calculated as:

$$m_{a1} = 0.2248kg$$

$$k_{a1} = 3549.9N/m$$

$$c_{a1} = 0.2825Ns/m$$

$$m_{a2} = 0.2804kg$$

$$k_{a2} = 17703N/m$$

$$c_{a2} = 0.7048Ns/m$$

4.2.4.2 Analytical Results

The absorber system is attached to the end of the cantilever beam, counteracting the applied excitation Z-force. The mass, stiffness and damping matrices of the absorber systems are incorporated into the Lumped Parameter model of the cantilever beam already analysed and proven in Section 2.1.1. From Figure 4.2-4, the transfer functions are very similar, proving the effectiveness of 1DOF (one degree of freedom system) to predict the response of the actual beam. The response of the effective system, however, has a slight decrease in amplitude, compared to the beam response over the selected low frequency range. This is expected because the 1DOF system response is based only on the first mode shape, whereas the response of the beam is based on the combination of mode shapes, of sin, cos, sinh and cosh functions. The design assumption is therefore assumed applicable to this structure.

Figure 4.2-5, shows the comparison between the beam and beam/absorber system transfer functions. The anti-resonance peaks of the beam/absorber system are, as expected, shifted to the driving frequencies of the applied Z-force and significantly reduced.

From the results obtained, the design procedures and optimisation process of the absorber design parameters significantly reduced the responses at the 1/rev and 2/rev frequencies of the applied force. The evaluation process is assumed effective and can be used when designing a similar absorber for the Finite Element tail boom, ensuring that the single degree of freedom model responds accurately with the first mode of the tail boom and the absorber components are optimised appropriately.

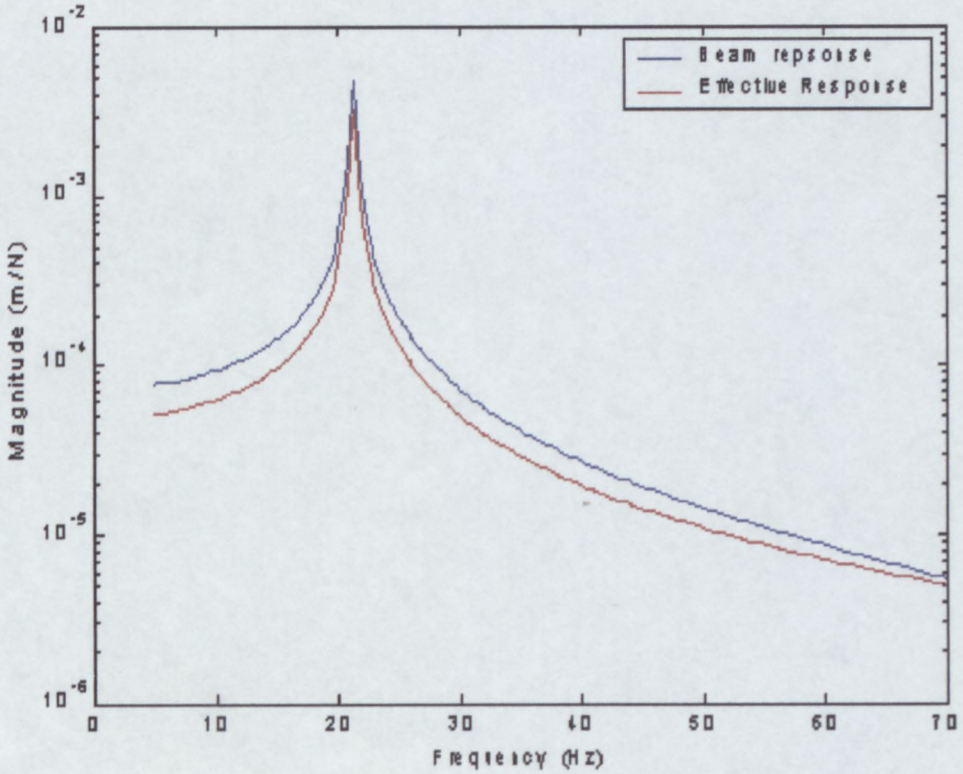

Figure 4.2-4: Response comparison between the 1DOF and BEAM systems

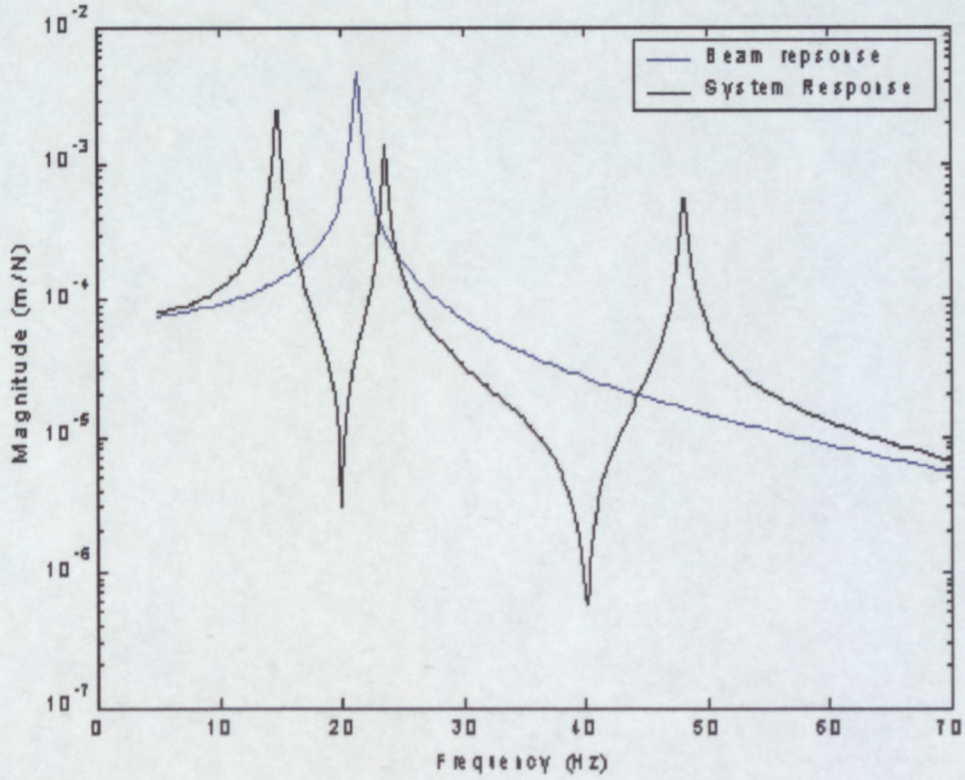

Figure 4.2-5: Transfer Function Comparison between the BEAM and BEAM/ABSORBER system

4.2.5 Finite Element Tail Boom Suppression System

The first mode shape of the FE tail boom model is considered the lateral bending mode. This mode can be related to the first bending mode shape of a simple beam structure. The derivation of the effective components used in section 4.2.4-1, are therefore assumed applicable to the calculation of the components of a FE tail boom absorber system. The optimised absorber design parameters corresponding to the tail boom structure are therefore calculated as:

$$m_{a1} = 0.4618kg$$

$$k_{a1} = 7292.4N/m$$

$$c_{a1} = 0.5803Ns/rad$$

$$m_{a2} = 0.5426kg$$

$$k_{a2} = 34278N/m$$

$$c_{a2} = 1.3638Ns/rad$$

4.2.5.1 Finite Element Absorber Model

The dynamic mass-springs-damper absorbers are modelled using the MASS and SPRING-elements of the NASTRAN library. The absorbers are connected to the hub of the tail boom using rigid links with all six degrees of freedom fixed.

4.2.5.2 Analytical Results

Simulations are run in NASTRAN using a modal dynamic frequency technique to analyse the transfer functions. Figure 4.2-6 shows the correspondence between the transfer functions of the 1DOF system and the Finite Element tail boom model. The comparison proves that at the lower frequency ranges, the FE tail boom is fairly accurately predicted by the 1DOF system. Thus the absorber system design procedure is applicable.

Figure 4.2-7 illustrates the absorber effect on the transfer function of the tail boom. At the excitation frequencies of 20 and 40 Hz, the response is reduced, proving the effectiveness of the suppression system design.

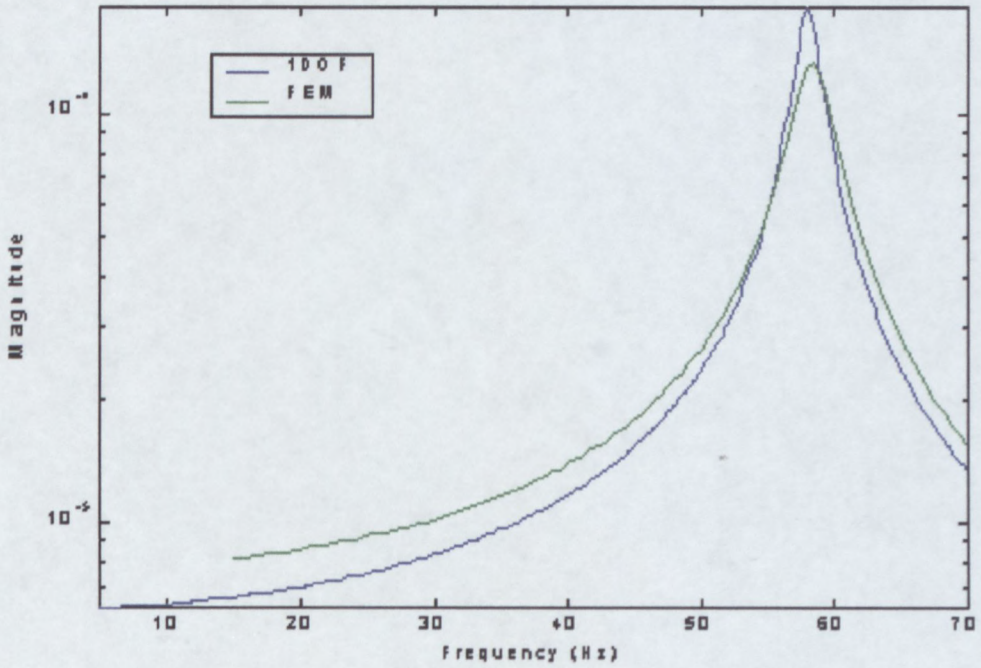

Figure 4.2-6: Response Comparison of 1DOF and FEM Tail Boom Systems

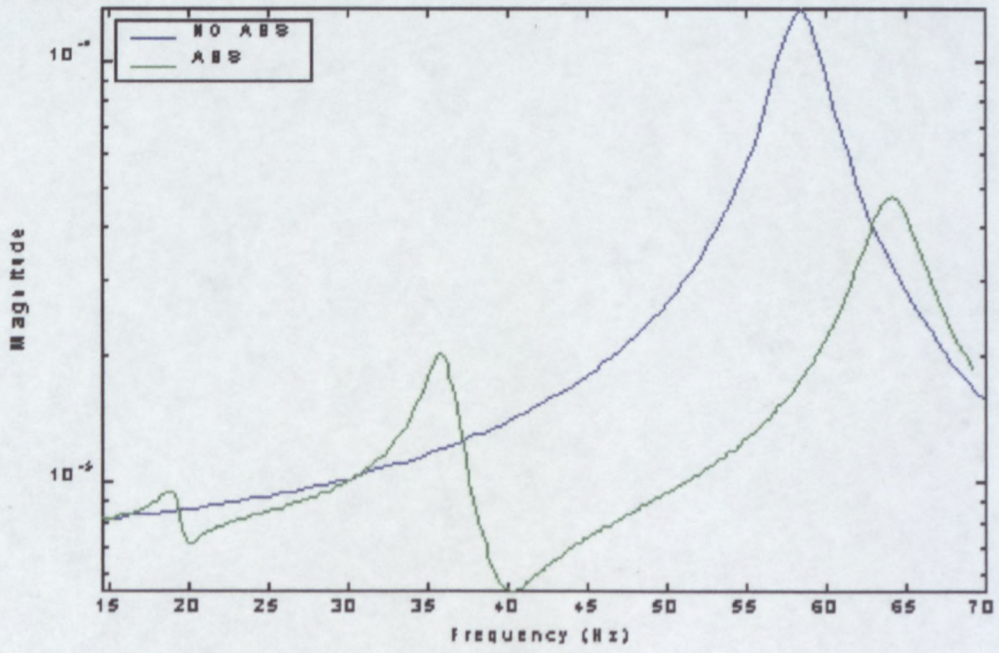

Figure 4.2-7: Transfer Function of Absorber Effectiveness

5 POSSIBLE RESEARCH APPLICATIONS

Two possible applications of the research presented in this thesis are discussed. The first application is the design and development of a complex vibration monitoring system. The second application is the use of the vibration suppression absorber responses to indirectly calculate the magnitudes of the excitation forces on the tail boom.

5.1 SIMPLIFIED MONITORING SYSTEM

An important aspect of helicopter safety is the monitoring of vibration responses and the incorporation of exceedence functions to warn the pilot of excessive vibrations caused by tail rotor dynamics. This has led to the development of a Health and Usage Monitoring System (HUMS), which is incorporated into most newly developed military and commercial helicopters. Helicopter HUMS were initially developed as a vibration monitoring technique and subsequently, the implementation of HUMS is also used to improve the airworthiness of helicopters. Certain parameters are monitored and any exceedence over an acceptable threshold is reported. This in itself assists in maintaining aircraft structural integrity through reducing vibration levels through constant monitoring of rotor systems and allowing preventative maintenance to be taken before vibration levels become damaging.

From the configurations and requirements of a fully integrated HUMS presented by Muldoon & Gill[16], Blunt, O'Neill & Rebbechi[17] and Trammell[18], the structure of a simplified monitoring system is shown in Figure 5.1-1.

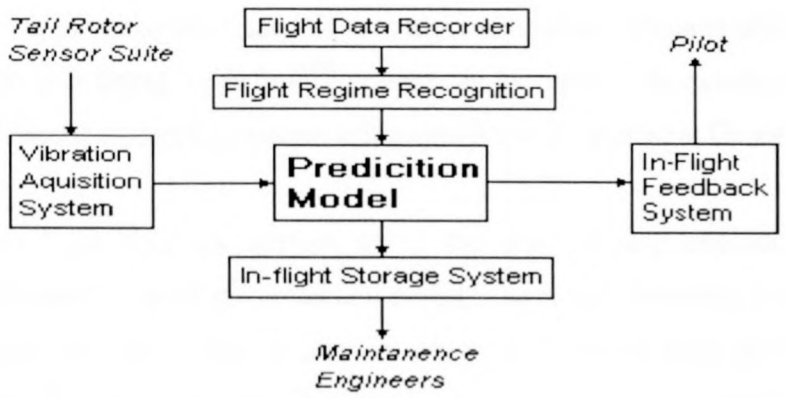

Figure 5.1-1: Simplified HUMS-based monitoring configuration

The system is designed around an exceedence prediction model, which compares experimentally measured vibration levels, corresponding to different flight regimes, to configurable exceedence limits. These allow comparisons of the levels of tail boom vibrations to determine excessive vibrations caused by damaged blades and bearing or gear wear.

The appropriate vibration limits are calculated from a large amount of in-flight vibration data, which is a costly and time-consuming process. Analytical results calculated from an effective model of the tail boom and tail rotor, could be a likely alternative to developing these vibration limits. The analytical solutions represent an ideal situation and therefore may provide a good baseline from which any exceedence can be measured. It is however questionable to assume that excitation forces under normal conditions can be predicted accurately by an analytical model, not to mention the response of the tail boom to these excitation forces. To develop an analytical model that predicts these trends reliably would be of great advantage and could be proposed as a challenging research topic.

The tail rotor sensor suite is mounted on the tail section to provide raw vibration and torque data required by the prediction model. These signals are acquired by the vibration acquisition system, which continuously checks the vibration data for irregularities and processes raw vibration data into suitable data signals and power averages.

The flight recorder specifies the flight parameters, such as, forward flight velocity, yaw rate, pitch rate etc, required as inputs into the flight regime recognition module. The flight regime recognition module uses algorithms to determine in which flight regime the helicopter is flying. Crawford[22] presents an example of an existing flight recorder and flight regime recognition system using algorithms developed at Georgia Tech.

The in-flight feedback system warns the pilot of any exceedence based on the configurable limits of the prediction model. The system provides a visual interface with the pilot using the cockpit display, on which, the type and duration of the exceedence is shown. The visual warning is cleared only by physically acknowledgement from the pilot.

As an example, Tail rotor vibrations at specific frequencies, along with corresponding causes and corrective actions are taken from the maintenance manual for the 5-bladed tail rotor SAAF ORYX and given in table 5.1-1.

Vibration Measured	**Possible Causes**	**Check and Corrective Action**
1/rev tail rotor	1. Tail Rotor Unbalance	Check and correct the unbalance
	2. Condition of Tail Rotor Blades	Check the condition of each blade, make repairs or replace defective blade
	3. Condition of Tail Rotor Transmission	Check for play, tightening, brinelling and greasing. Check the torque load of the tail rotor attachment bolts
	4. Rigging of Tail Rotor Controls	Check and re-rig if necessary
5/rev tail rotor	1. Tail Rotor Control	Check the servo-controls and adjust if necessary

Table 5.1-1: SAAF ORYX Tail Rotor Vibration Maintenance Chart

The in-flight storage system, stores all necessary data, including vibration signals and averages, exceedence, flight parameters and flight regimes and the time within these regimes etc. The storage system allows post flight interfacing with the maintenance engineers if severe vibrations are detected.

The configuration and basic requirements for the development of a simple monitoring system are introduced to provide a basic idea of what components a working model would require. The manufacture and implementation of such a system on an actual tail boom requires a more detailed investigation into existing and allowable components, which is outside the scope of this thesis. The development of such a monitoring system could make for a challenging research project.

5.2 FORCE MAGNITUDE MEASURING SYSTEM

To test the accuracy of the tail boom analytical model an accurate representation of the forces applied at the critical areas during all flight regimes is required. Accurately predicting the aerodynamic forces under normal conditions using an analytical model of any tail rotor is unlikely and measuring these forces during flight is a challenging task. Tail booms modified with the double anti-resonance absorber, designed in this study, may help to solve this problem.

A measurement of the magnitudes of the two dominant excitation forces applied at the hub position of the tail rotor may be indirectly calculated from the measured response of the individual vibration absorber masses. The transfer functions for the designed dynamic vibration absorbers, applied to the Finite Element model of the tail boom are shown in Figure 5.2-1. At the 1/rev-excitation frequency, 20 Hz, the vibration response of the 1/rev absorber is shown to be significantly larger when compared to the response of the 2/rev absorber. The 2/rev-vibration absorber at the 2/rev-excitation frequency, 40Hz, also indicates at this trend. Thus, the 1/rev-and 2/rev absorber mass responses are assumed to cancel the major magnitudes of 1/rev and 2/rev-excitation force respectively. It may therefore be possible to indirectly calculate the magnitude of the 1/rev and 2/rev excitation frequencies by individually measuring the vibration responses of the of the 1/rev and 2/rev dynamic absorbers.

The results presented are limited to the analysis of tail boom vibrations caused by excitation forces in-line with the thrust of a two-bladed tail rotor, as researched in this thesis. This indirect method of measuring forces using absorber mass responses requires extensive experimental testing to ensure the effectiveness of the assumptions. However the experimentation falls outside the scope of this thesis, but may provide an interesting research topic for further investigation.

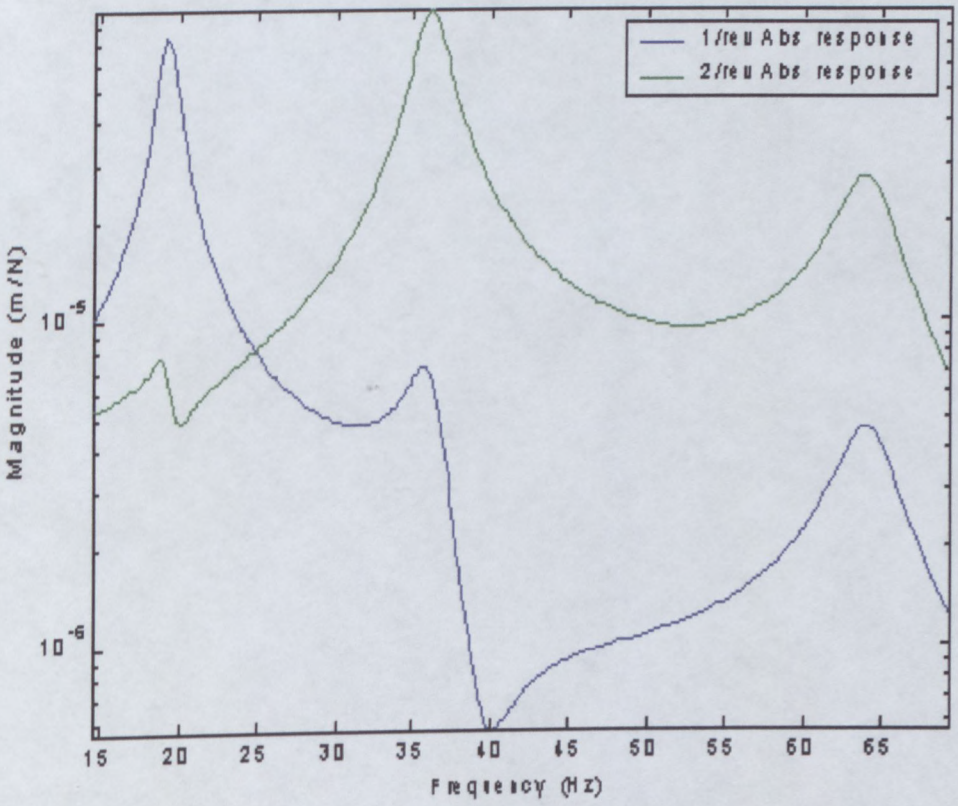

Figure 5.2-1: 1/rev and 2/rev Absorber Response Transfer Functions

6 CONCLUSION

An experimental investigation was conducted using a cantilever beam to illustrate an understanding of vibration techniques and phenomena. The free and forced vibration of the cantilever beam was investigated using various modelling strategies. Theoretical models such as the Lumped parameter, Myklestad, Distributed Parameter and Finite Element Methods were analysed and compared with experimental measurements. Excellent agreement of the natural frequencies, mode shapes and the harmonic transfer functions were found. The results prove the accuracy of all four modelling strategies and of the calculation of the experimental damping ratios and mode shapes from the experimental measurements. The analysis gives a thorough background into vibration analysis techniques and highlights the most important vibration phenomena.

To investigate the vibrations of helicopter tail sections, a Finite Element Method was selected to model a simplified design of a helicopter tail boom. The Finite Element model was tested against experimental data and the results correlated accurately, proving the effectiveness of the model. The Finite Element model was used to predict tail boom responses during specific flight patterns and to evaluate the effectiveness of vibration suppression systems without the necessity of in-flight or experimental testing.

A vibration suppression system for reducing tail boom vibrations at its two dominant frequencies was designed and tested on the Finite Element Model. The suppression system was designed using two, parallel dynamic absorbers. For the purposes of this thesis, the dynamic absorbers were tuned to reduce the resonant peaks at the dominant excitation frequencies of the excitation force in-line with the thrust of the tail rotor only.

This excitation force exerted on the tail boom was estimated using a simplified tail rotor dynamic model. The estimation when compared with actual vibration data was assumed to predict the basic frequency trends of the forces, reliably.

Incorporating the designed components into an accurate Lumped Parameter model of a cantilever beam structure and simulating the response of the structure at the dominant excitation frequencies of the calculated excitation force tested the vibration suppression system. The results were obtained from meticulously following the optimisation procedure and it is believed therefore that the investigation proves the effectiveness of the design procedure and optimisation process of the design parameters.

A similarly designed suppression system was incorporated into the Finite Element tail boom model and from the analytical results obtained, the suppression system was shown to cause a fair reduction in the vibration response at the two dominant frequencies of the excitation force.

Finally, two possible applications were suggested from the research presented in this thesis. The first application was the development of a simplified vibration monitoring system for the helicopter tail boom. A simplified configuration of a vibration monitoring system for the tail boom was presented to give a basic idea of the components and requirements of such a system. The second application was the possible development of a system using the response of vibration suppression absorbers to predict the magnitudes of the excitation forces on the tail boom.

7 REFERENCES

1. Loewy, R.G., ***'Helicopter Vibrations: A Technological Perspective'***, Alexander A. Nikolsky Honorary Lecture, 40th annual Forum of the American Helicopter Society, Arlington. Virginia, May 1984.

2. Ewins, D.J., ***'Modal Testing: Theory and Practice'***, Research Studies Press, Taunton, Somerset, England, 1984

3. Tse, F.S., Morse, I.E. & Hinkle, R.T., ***'Mechanical Vibrations: Theory and Applications'***, 2nd edition, Allyn and Bacon, Inc, Boston, Massachusetts, 1978

4. Meirovich, L, ***'Principles and Techniques of Vibrations'***, Prentice Hall, New Jersey, 1997

5. Inmann, D.J., ***'Engineering Vibration'***, Prentice Hall, New Jersey, 1996

6. Rossit, C.A. & Laura, P.A.A., ***'Free Vibrations of a Cantilever Beam with a Spring-Mass System at the Free End'***, Ocean Engineering, Volume 28, 933-939, 2001

7. Low, K.H., ***'Comparisons of Experimental and Numerical Frequencies for Classical Beams carrying a Mass in-span'***, International Journal of Mechanical Sciences, Volume 41, 1515-1531, 1999

8. Cook, R.D., Malkus, D.S. & Plesha, M.E., ***Concepts and Applications of Finite Element Analysis***, 3rd edition, John Wiley & sons, New York, 1989

9. Fledel, S., Rand, O. & Chopra, I., ***'Coupled Rotor/Airframe Vibration Analysis'***, Fifteenth European Rotorcraft Forum, Paper No. 52, Amsterdam, The Netherlands, September 1989

10. Yeo, H. & Chopra, I., ***'Coupled rotor/fuselage vibration analysis using detailed 3-D airframe models',*** Mathematical and Computational Modelling, Volume 33, Issues 10-11, 1035-1054, May-June 2001

11. Bramwell, A.R.S., '***Helicopter Dynamics'***, Edward Arnold, The City University, London, 1976

12. Gessow, A. & Myers, G.C, '***Aerodynamics of the Helicopter'***, Frederick Ungar Publishing co., New York, 1967

13. Greenwood, D.T., ***'Principles of Dynamics'***, 2nd edition, Prentice Hall, New Jersey, 1988

14. Cha, P.D. & Pierre, C., ***'Frequency analysis of a linear Elastic Structure Carrying a Chain of Oscillators'***, Journal of Engineering Mechanics, Volume 125, Issue 5, 587-591, May 1999

15. Aida, T., Toda, S., Ogawa, N. & Imada, Y., ***'Vibration control of Beams using Beam-type Dynamic Vibration Absorbers'***, Journal of Engineering Mechanics, Volume 118, No. 2, 248-258, February 1992

16. Muldoon, R. & Gill, J., ***'U.S. Navy / BFGoodrich Integrated Mechanical Diagnostics HUMS Overview & Status'***, Workshop on Helicopter Health and Usage Monitoring Systems – part 2, Melbourne, Australia, February 1999

17. Blunt, D, O'Neill, P & Rebbechi, B, ***'Vibration Monitoring of Royal Australian Navy Helicopters'***, Workshop on Helicopter Health and Usage Monitoring Systems, Melbourne, Australia, February 1999

18. Trammel, C, ***'UK Ministry of Defence Health and Usage Monitoring System (HUMS)'***, Workshop on Helicopter Health and Usage Monitoring Systems, Melbourne, Australia, February 1999

19. Yin, J.P. & Ahmed, S.R., ***'Helicopter Main-Rotor/Tail-Rotor Interactions'***, Journal of American Helicopter Society, Vol. 45, Issue 4, 293-302, October 2000

20. Basset, P.M. '***Modelling of the dynamic inflow on the main rotor and tail rotor components in Helicopter flight mechanics'***, Annual Forum Proceedings – American Helicopter Society, Vol 2, 1643-1656, 1997.

21. Vanderplaats, G.N., ***'Numerical Optimisation techniques for engineering design'***, 3rd edition, Prentice Hall, New Jersey,1999

22. Crawford, C, ***'HH-60G Mission Usage Spectrum Survey: Methodology Overview'***, Workshop on Helicopter Health and Usage Monitoring Systems, Melbourne, Australia, February 1999

23. Shigley, J.E. & Mischke, C.R, ***'Mechanical Engineering Design'***, 5th edition, McGraw-Hill Book Company, 1989

24. Greenberg, M,D, ***'Advanced Engineering Mathematics',*** 2nd edition, Prentice Hall, New Jersey, 1998

APPENDIX A

VIBRATION ANALYSIS

A.1 CALCULATION OF TORSIONAL SPRING STIFFNESS

For a cantilever beam, using simple beam theory derived in Shigley & Mischke [23], the upward deflection w caused by a downward force applied at the end of the beam is given at a distance x from the clamped end as

$$w = \frac{fx^2}{6EI}(x - 3l) \qquad \text{[A.1-1]}$$

For a rigid beam attached to a torsional spring, the static deflection is defined using the torsional spring equation $M = K_t\theta$. Hence the deflection caused by a force applied at the end of the beam is derived at a distance x along the length l as:

$$w = -\frac{flx}{K_t} \qquad \text{[A.1-2]}$$

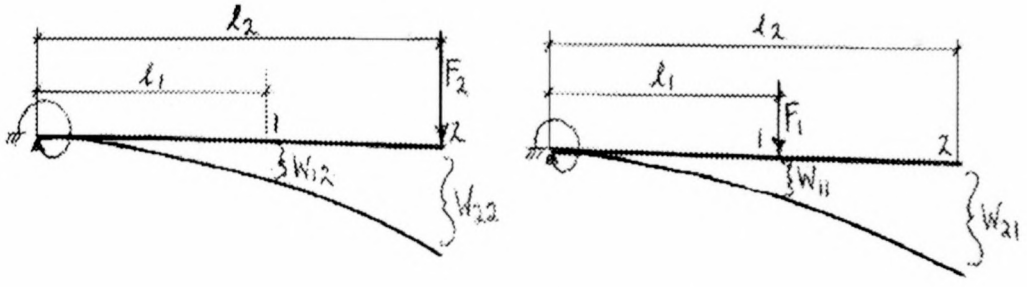

Figure A.1-1: Static Deflection Measurements

Measuring the deflections w as shown in Figure A.1-1, the equations combine into matrix form as:

$$\overline{w} = [S]\overline{z} \qquad \text{[A.1-3]}$$

$$\overline{w} = \begin{bmatrix} w_{11} \\ w_{12} \\ w_{21} \\ w_{22} \end{bmatrix}$$

$$[S] = \begin{bmatrix} -\dfrac{F_1 l_1^3}{3} & -F_1 l_1^2 \\ \dfrac{F_2 l_1^2 (l_1 - 3l_2)}{6} & -F_2 l_1 l_2 \\ \dfrac{F_1 l_2^2 (l_2 - 3l_1)}{6} & -F_1 l_2 l_1 \\ -\dfrac{F_2 l_2^3}{3} & -F_2 l_2^2 \end{bmatrix}$$

$$\bar{z} = \begin{bmatrix} \dfrac{1}{EI} \\ \dfrac{1}{K_t} \end{bmatrix}$$

The solution for the effective EI and K_t values are obtained using the least squares method for solution of the over determined matrix, defined as

$$\bar{z} = \left([S]^T [S] \right)^{-1} [S]^T \bar{w} \qquad \textbf{[A.1-4]}$$

A.2 DERIVATION OF FLEXIBILITY MATRIX

The flexibility matrix $[A]$ is based on the derivation of the influence coefficients a_{ij} of the beam structure, where

$$\overline{w} = [A]\bar{f} \qquad \text{[A.2-1]}$$

This requires the slender beam to be modelled as two separate structures: a cantilever beam and a rigid beam attached to a torsional spring at one end and the influence coefficients of each structure to be combined to form the overall flexibility matrix.

The influence coefficients for a cantilever beam b_{ij} are based on simple beam theory, derived in Shigley & Mischke [23], and are defined as

$$b_{ij} = \begin{cases} \dfrac{x_i^2\left(x_i - 3x_j\right)}{6EI} & i < j \\ -\dfrac{x_i^3}{3EI} & i = j \\ \dfrac{x_j^2\left(x_j - 3x_i\right)}{6EI} & i > j \end{cases} \qquad \text{[A.2-2]}$$

The influence coefficients for a rigid beam attached to a torsional spring c_{ij} are derived from the torsional spring properties $M = K_t\theta$ as

$$c_{ij} = -\frac{x_i x_j}{K_t} \quad i, j = 1,2,\ldots..,\ n \qquad \text{[A.2-3]}$$

The overall Influence coefficients of the flexibility matrix are therefore simply

$$a_{ij} = b_{ij} + c_{ij} \qquad \text{[A.2-4]}$$

A.3.1 Estimation of Modes Shapes

The determination of mode shapes form experimental data requires use of the measured transfer functions. The method assumes that the resonant peaks are not closely spaced and in the vicinity of peaks the frequency response is dominated by a single degree of freedom system for that mode.

From modal analysis of the basic equation of motion

$$[M]\ddot{\bar{x}}+[C]\dot{\bar{x}}+[K]\bar{x} = \bar{f}e^{j\omega_{dr}t} \qquad \text{[A.3-1]}$$

the transfer function is derived using modal summation as

$$[H]=\sum_{1}^{n}\hat{h}_i(\omega)[\bar{u}_i\bar{u}_i^T] \qquad \text{[A.3-2]}$$

$$\hat{h}_i(\omega) = \frac{1}{\hat{m}_i(\omega_{ni}^2-\omega_{dr}^2+j2\zeta_i\omega_{ni}\omega_{dr})}$$

the k-th column of the transfer function, associated with the eigen vector u_{kj} at the k-the point on the beam, is derived as

$$\bar{H}_k(\omega) = \hat{h}_1(\omega)u_{k1}\bar{u}_1+\ldots+\hat{h}_k(\omega)u_{kk}\bar{u}_k+\ldots+\hat{h}_n(\omega)u_{kn}\bar{u}_n \qquad \text{[A.3-3]}$$

Under the assumption of well spaced resonant frequencies, if $\omega = \omega_{nl}$, the l-th natural frequency, it can be shown that:

$$\left|\hat{h}_i(\omega_{nl})\right| << \left|\hat{h}_l(\omega_{nl})\right| \qquad \text{[A.3-4]}$$

thus

$$\bar{H}_k(\omega_{nl}) \approx \hat{h}_l(\omega_{nl})u_{kl}\bar{u}_l \qquad \text{[A.3-5]}$$

This equation is normalised as:

$$\bar{H}_k(\omega_{nl}) \approx \frac{\bar{u}_l}{\sqrt{\bar{u}_l^T\bar{u}_l}} \qquad \text{[A.3-6]}$$

The normalised eigenvectors can be obtained at any natural frequency in the system from the normalised magnitude of the transfer function measured at that peak frequency.

A.3.2 Derivation of Damping Ratios

The modal damping ratio is derived using the *3-dB point down* method derived in Inmann[5]. Let the points on the $\omega - axis$, where the magnitude of $H(\omega)$ is $3dB$ lower then at the damped natural frequency ω_d be ω_a and ω_b. Therefore:

$$|H(\omega_a)| = |H(\omega_b)| = |H(\omega_d)|/\sqrt{2} \qquad \textbf{[A.3-8]}$$

Assuming that the modal damping is small, frequencies at points *a* and *b* and the peak frequency yield an equation for deriving the modal damping ratios.

$$\zeta_i = \frac{\omega_a - \omega_b}{2\omega_{di}} \qquad \textbf{[A.3-9]}$$

The modal damping ratio is assumed to be proportional to the stiffness and mass of the system. Thus

$$[\hat{C}] = \alpha[\hat{M}] + \beta[\hat{K}] \qquad \textbf{[A.3-10]}$$

or in generalised form as:

$$2\zeta_i\omega_{ni} = \alpha + \beta\omega_{ni}^2 \qquad \textbf{[A.3-11]}$$

Using matrix formulation

$$[Q]\begin{bmatrix}\alpha\\ \beta\end{bmatrix} = [R] \qquad \textbf{[A.3-12]}$$

$$[Q] = \begin{bmatrix}1 & \omega_{n1}^2\\ . & .\\ 1 & \omega_{nn}^2\end{bmatrix}$$

$$[R] = 2\begin{bmatrix}\zeta_1\omega_{n1}\\ .\\ \zeta_n\omega_{nn}\end{bmatrix}$$

which can be used to determine the values for α and β which accurately define the damping at each resonance peak using a least squares fit.

A.4 ORTHOGONALITY RELATIONS OF EIGEN FUNCTIONS

For the *rth* and *sth* mode, the differential equations of free harmonic motion are derived as

$$-\omega_{nr}^2 m\varphi_r + EI\varphi_r'''' = 0 \qquad \text{[A.4-1]}$$

$$-\omega_{ns}^2 m\varphi_s + EI\varphi_s'''' = 0 \qquad \text{[A.4-2]}$$

Pre-multiplying equation by φ_s and integrating over the length of the beam, yields the equation:

$$\int_0^L \left(-\omega_{nr}^2 m\varphi_s\varphi_r + EI\varphi_s\varphi_r''''\right)dx = 0 \qquad \text{[A.4-3]}$$

Integrating twice by parts and substituting the boundary conditions of the system into the resulting equation, it follows that:

$$-\omega_{nr}^2\left(m\int_0^L \varphi_s\varphi_r dx + m_{tip}\varphi_s(L)\varphi_r(L)\right) + EI\int_0^L \varphi_s''\varphi_r'' dx + K_t\varphi_s'\Big|_{x=0}\varphi_r'\Big|_{x=0} = 0 \qquad \text{[A.4-4]}$$

Following the same procedure, only with φ_r the result is

$$-\omega_{ns}^2\left(m\int_0^L \varphi_r\varphi_s dx + m_{tip}\varphi_r(L)\varphi_s(L)\right) + EI\int_0^L \varphi_r''\varphi_s'' dx + K_t\varphi_r'(0)\varphi_s'(0) = 0 \qquad \text{[A.4-5]}$$

Subtracting equation A.4-4 from equation A.4-5, and since $\omega_r \neq \omega_s$, the orthogonal relations of the beam equation are derived as:

$$m\int_0^L \varphi_s\varphi_r dx + m_{tip}\varphi_s(L)\varphi_r(L) = 0 \qquad \text{for} \quad r \neq s \qquad \text{[A.4-6]}$$

$$EI\int_0^L \varphi_r''\varphi_s'' dx + K_t\varphi_r'(0)\varphi_s(0) = 0 \qquad \text{for} \quad r \neq s \qquad \text{[A.4-7]}$$

A.5 SLENDER BEAM PROPERTIES

Elastic Isotropic Material Properties

$E = 209GN/m^2$

$\nu = 0.3$

$\rho = 7800kg/m^3$

Slender Beam Properties

$l = 1m$

$I_{xx} = I_{yy} = I_{eff} = 3.274x10^{-8}m^4$

$A = 3.2x10^{-4}m^2$

$\varsigma_1 = 0.0147$

$\varsigma_2 = 0.0056$

$\alpha = 1.8988rad/s$

$\beta = 3.794x10^{-6}s/rad$

Clamping Stiffness

$K_t = 40510Nm/rad$

A.6 EXPERIMENTAL TEST SET-UP AND EQUIPMENT

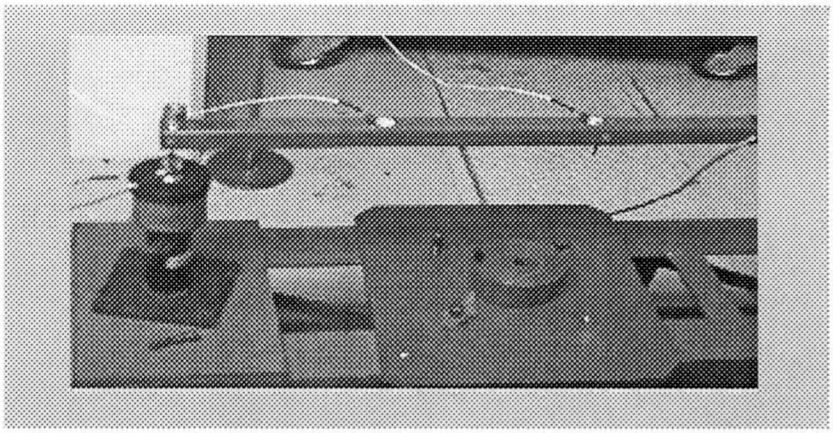

Figure A.6-1: Accelerometer and Shaker Set-up for Slender Beam Analysis

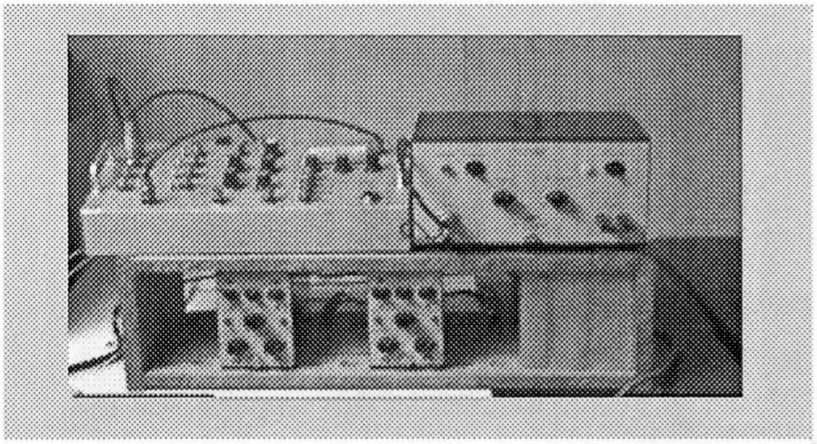

Figure A.6-2: Force and Charge Amplifier Set-up

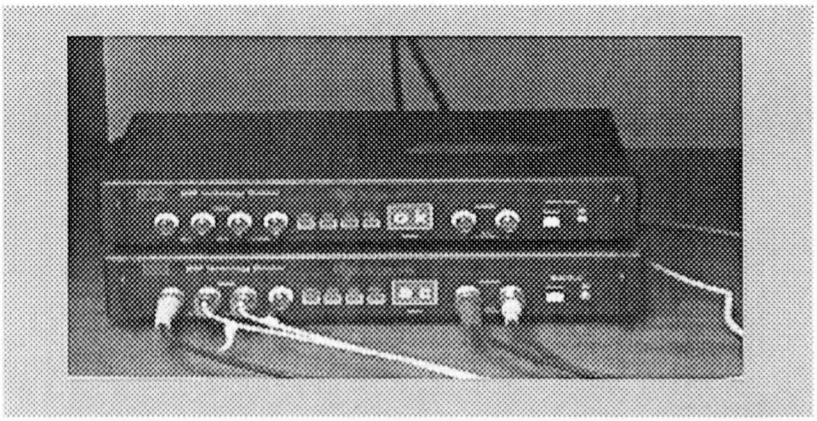

Figure A.6-3: DSP SIGLAB System Set-up

APPENDIX B

TAIL BOOM TEST EQUIPMENT AND SET-UP

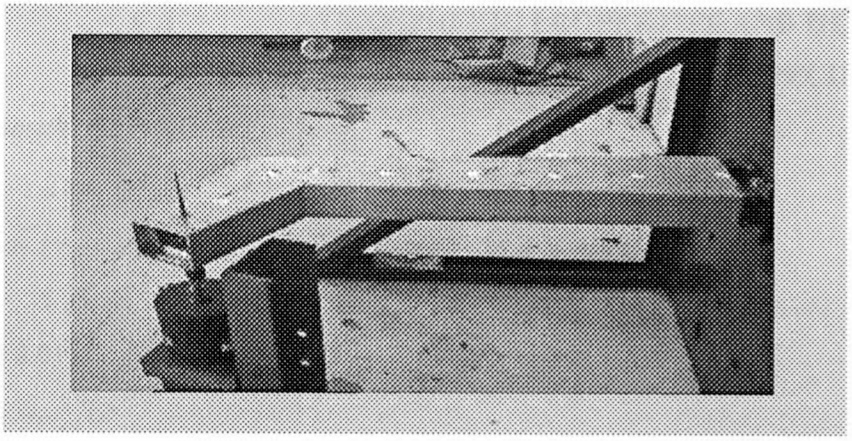

Figure B.1-1: Tail Boom Test Structure

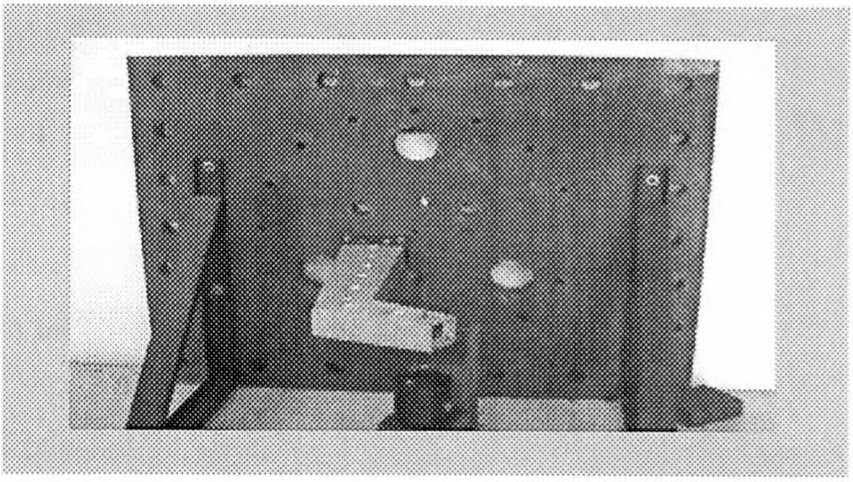

Figure B.1-2: Tail Boom Fixture

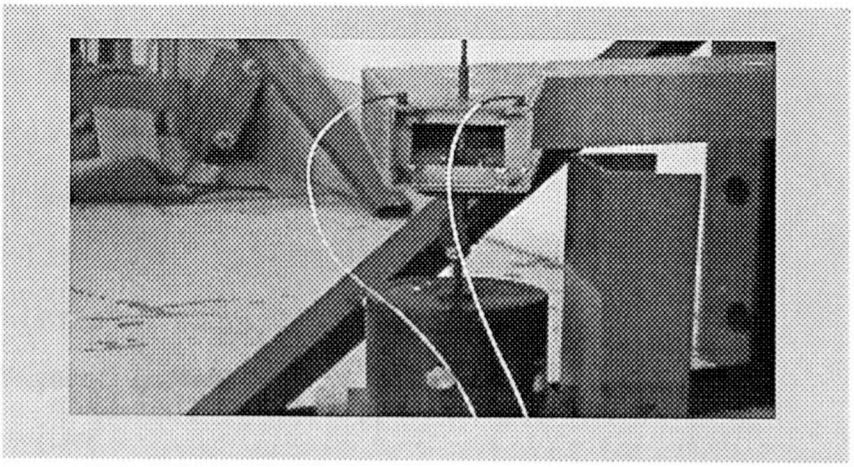

Figure B.1-3: Tail Boom Accelerometer and Shaker Set-up

APPENDIX C

TAIL ROTOR DYNAMICS

C.1 ATMOSPHERIC PROPERTIES AND HELICOPTER SPECIFICATIONS

Atmospheric Properties

$\rho = 1.2\,kg/m^3$

Blade Properties and Inertial Properties (for a lamina)

$a = 5.5$

$\delta = 0.013$

$A = m_b c^2/12$

$B = m_b R_b^{\,2}/12$

$C = A + B$

Main Rotor

$b_{mr} = 4$

$m_b = 74kg$

$r_{cg} = 4m$

$c = 0.3m$

$R_b = 7.5\,m$

$N = 240rpm$

Tail rotor

$b_{tr} = 2$

$M_b = 4kg$

$r_{cg} = 0.7m$

$c = 0.2m$

$R_b = 1.5m$

$N = 1200rpm$

Helicopter Properties

$Do = 2.3m^2$

$W = 45000N$

C.2 SAAF ROTORTUNE VIBRATION DATA

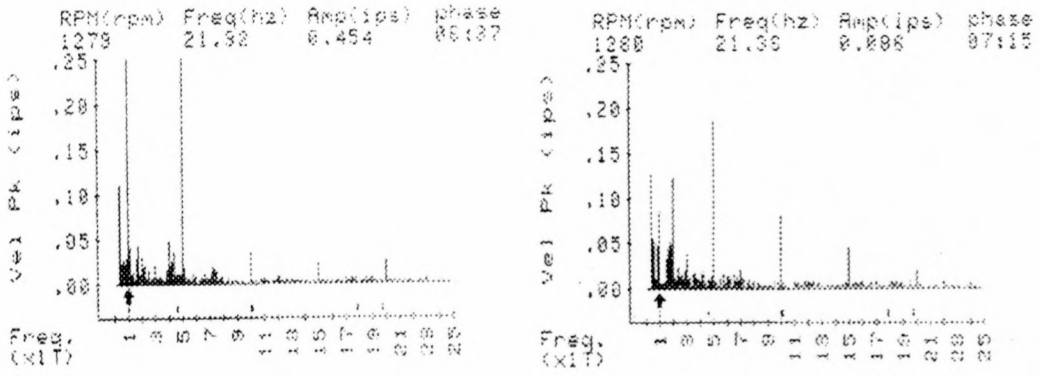

Figure C.2-1: Tail rotor Lateral Vibration in Forward Flight (110kts)

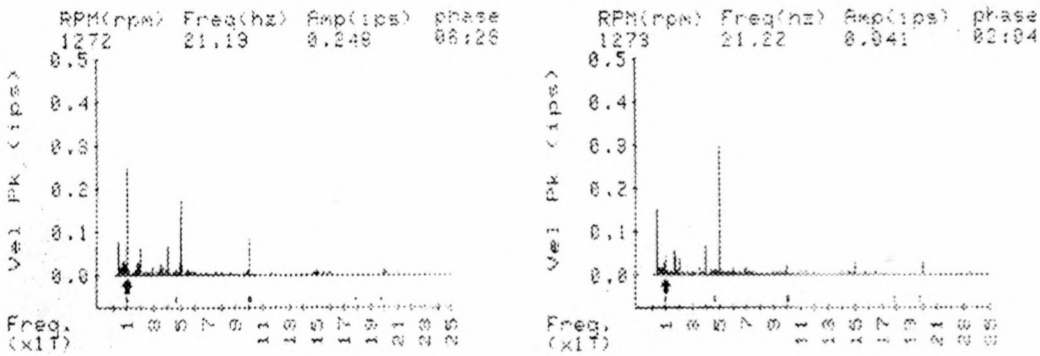

Figure C.2-2: Tail rotor lateral Vibration in Hover